WAVEFUNCTION EFFECTS IN INNER SHELL IONIZATION OF LIGHT ATOMS BY PROTON

Kjell Aashamar and Per Amund Amundsen
Institute of Physics
University of Oslo, Norway

Report 80-10

WAVEFUNCTION EFFECTS IN INNER SHELL IONIZATION OF LIGHT ATOMS BY PROTONS.

KJELL AASHAMAR AND PER AMUND AMUNDSEN
INSTITUTE OF PHYSICS
UNIVERSITY OF OSLO, NORWAY.

Abstract.

An efficient computer code for calculating the impact parameter distribution of atomic ionization probabilities caused by charged particle impact, has been developed. The programme is based on the semiclassical approximation, and it allows the use of an arbitrary atomic central potential for deriving the one-electron orbitals that form the basis for the description of the atomic states.
Extensive calculations are reported for proton induced K-shell ionization in carbon and neon, covering energies in the range 0.1-10 MeV. Some calculations on proton-argon L-shell ionization are also reported. Comparison of the results obtained using (screened) hydrogenic potentials and the recently reported energy-optimized effective atomic central potentials, respectively, demonstrates that wavefunction effects are generally important for inner-shell ionization of light atoms.
The agreement between theory and experiment in the K-shell case is improved for fast collisions upon using better wavefunctions.

1. Introduction.

The impact parameter distribution of the inner-shell ionization probability in ion atom collisions has proved a useful tool for investigating the ionization mechanism. As most experiments till now have been carried out at relacively low collision energies, when the projectile mostly interacts with the innermost part of the atomic wavefunctions, agreement with theoretical calculations using (possibly relativistic) hydrogenic wavefunctions has been very satisfactory (Lægsgaard & al. 1978). Recently, however, measurements have been extended to collisions where the projectile moves at speeds somewhat larger than the target electrons (Horsdal-Pedersen et al. 1979). In this energy region it has been known since long from calculations of total cross-sections in the plane wave Born approximation (PWBA) that the influence of the other (spectator) electrons on the wavefunctions of the ejected electron cannot be neglected (Arthurs 1959).

Till now only a few calculations of the ionization probability as a function of impact parameter in the semiclassical approximation (SCA) with non-hydrogenic wavefunctions have been reported (Aashamar and Kocbach 1977, Pauli et al. 1978, Bauer et al. 1978). These calculations cover only a very limited range of collision systems and energies.

In order to investigate the wavefunction effects in more detail, we have developed an efficient computer code for calculating SCA ionization probabilities with electronic wavefunctions evaluated in an arbitrary central potential. In the present paper, we present calculations of K and L shell ionization of light atoms by fast protons, where straight line SCA with non-relativistic wavefunctions is applicable.

It may of course be argued that at such high energies, the Bohr (1948) criterion for a classical projectile description to be valid is not, or only marginally, fulfilled. On the other hand, except for large projectile

scattering angles, the angular momentum of the projectile will be quite large, so that if the ionisation probability is not found to vary very rapidly with scattering angle, the semiclassical approximation should be justified.

In section 2 we outline the SCA theory for many-electron systems in the momentum representation, which is the basis of the present calculations. For straight line SCA, Bang and Hansteen (1959) in their original paper on the SCA, gave an explicit expression for the transition operator in coordinate representation. However, they used cartesian coordinates, and transformation to spherical coordinates, which is more convenient for numerical work, is not straightforward. In section 3 we therefore give an explicit expression for the multipole expansion of the transition operator in coordinate space. Although these expressions are not well suited for numerical work, they are useful for interpreting the numerical results.

In section 4 we outline our numerical procedures, the results are presented in section 5, and section 6 finally summarizes the conclusions. The actual derivation of the transition operators is outlined in an appendix.

Atomic units ($e = m_e = \hbar = 1$) are used throughout this paper, unless otherwise indicated.

2. Theory - momentum space formulation.

We consider a system consisting of a charged particle of mass M_1, charge Z_1, energy E_1, and velocity v_1 which is scattered off an N-electron atom or ion of nuclear charge Z_2. The scattering process may be accompanied by a change of state of the atomic system, and we want to determine the probabilities for the different transitions possible.

In the semiclassical approximation (SCA) or impact parameter method one assumes that the projectile can be treated as a classical particle and its motion described in terms of a classical trajectory $\underset{\sim}{R}_b(t)$ associated with an impact parameter b (see Fig. 1). This is a valid and reasonable approximation as long as the de Broglie wavelength of the projectile is (much) smaller than the distance of closest approach. At the same time it should be large enough for interference effects to be negligible, thereby allowing a given scattering angle to be associated with a definite value of the impact parameter. Moreover, in the present paper we assume that the masses involved are such that we can neglect recoil of the target atom, and hence anchor our system of reference to the target atom nucleus. We shall further limit our discussion to projectile energies for which $v_1 \ll c$, c being the velocity of light, and we also neglect relativistic effects in our description of the target atom.

Having thus spelled out the various approximations and limitations, we are left with a time-dependent model atomic Hamiltonian

$$H(t) = H_o + H_1(t) \ , \tag{2.1}$$

where

$$H_o = \sum_{k=1}^{N} h(k) + \sum_{k<\ell} g(k,\ell) \ , \tag{2.2}$$

$$h(k) = -\frac{1}{2}\nabla_k^2 - Z_2/r_k \ , \quad g(k,\ell) = 1/r_{k\ell} \ , \tag{2.3}$$

and

$$H_1(t) = -\sum_{k=1}^{N} Z_1/|\underset{\sim}{r}_k - \underset{\sim}{R}_b(t)| \xrightarrow[t\to\pm\infty]{} 0. \tag{2.4}$$

Assuming a set of mutually orthogonal (and normalized) one-electron spin-orbitals $\{\phi_k\}$, and adopting the single-determinant approximation, we may represent the zeroth-order atomic states by wavefunctions

$$\Psi_i = C_i \, \mathrm{Det}\{\phi_1(1) \ldots \phi_i(i) \ldots \phi_N(N)\}, \tag{2.5}$$

where C_i is a normalization constant.

The corresponding energy is given by

$$E_i = \langle \Psi_i | H_o | \Psi_i \rangle . \tag{2.6}$$

Since H_1 is basically a one-electron operator and the orbitals ϕ_k are assumed orthogonal, H_1 can cause first-order transitions only between states Ψ_i and Ψ_f which differ in a single orbital. With Ψ_i as given in Eq. (2.5) representing the initial state we therefore consider final states of the form

$$\Psi_f = C_f \, \mathrm{Det}\{\phi_1(1) \ldots \phi_f(i) \ldots \phi_N(N)\}, \tag{2.7}$$

where

$$E_f = \langle \Psi_f | H_o | \Psi_f \rangle . \tag{2.8}$$

The first-order probability amplitude a_{fi} for the transition $i \to f$ is then given by

$$a_{fi} = -\frac{i}{\hbar} \int_{-\infty}^{\infty} dt \; e^{i\omega t} \langle \Psi_f | H_1(t) | \Psi_i \rangle , \tag{2.9}$$

where

$$\omega \equiv \omega_{fi} = (E_f - E_i)/\hbar . \tag{2.10}$$

The matrix element of H_1 reduces to a simple one-electron integral

$$\langle \Psi_f | H_1(t) | \Psi_i \rangle = - \langle \phi_f | Z_1/|\underset{\sim}{r} - \underset{\sim}{R}_b(t)| | \phi_i \rangle , \tag{2.11}$$

and for the energy difference we have

$$E_f - E_i = \sum_{k\neq i} \langle\phi_k|h|\phi_k\rangle + \sum_{\substack{k<\ell \\ k,\ell\neq i}} [\langle\phi_k\phi_\ell|g|\phi_k\phi_\ell\rangle - \langle\phi_k\phi_\ell|g|\phi_\ell\phi_k\rangle]$$

$$- \sum_{k\neq f} \langle\phi_k|h|\phi_k\rangle - \sum_{\substack{k<\ell \\ k,\ell\neq f}} [\langle\phi_k\phi_\ell|g|\phi_k\phi_\ell\rangle - \langle\phi_k\phi_\ell|g|\phi_\ell\phi_k\rangle]$$

$$= \epsilon_f + E_B , \tag{2.12}$$

where

$$E_B = - \langle\phi_i|h|\phi_i\rangle - \sum_{k\neq f} [\langle\phi_k\phi_i|g|\phi_k\phi_i\rangle - \langle\phi_k\phi_i|g|\phi_i\phi_k\rangle] \tag{2.13}$$

is the binding energy associated with ϕ_i in state Ψ_i if relaxation effects are neglected.

Correspondingly,

$$\epsilon_f = \langle\phi_f|h|\phi_f\rangle + \sum_{k\neq i} [\langle\phi_k\phi_f|g|\phi_k\phi_f\rangle - \langle\phi_k\phi_f|g|\phi_f\phi_k\rangle] \tag{2.14}$$

$$\approx \langle\phi_f|h|\phi_f\rangle ,$$

where the last (approximate) equality is based on the assumption that the orbital ϕ_f is well separated in space from all other orbitals ϕ_k involved. In particular, if ϕ_f is a continuum orbital, whereas all the other one-electron states are bound, the equality is exact.

Using one-electron orbitals of the form

$$\phi_k = R_{n\ell}(r)\, Y_{\ell m}(\hat{r})\chi_\mu(\sigma) \tag{2.15}$$

and noting that

$$1/|\underset{\sim}{r} - \underset{\sim}{R}| = \frac{1}{2\pi^2} \int d^3s\, s^{-2}\, e^{i\underset{\sim}{s}\cdot(\underset{\sim}{r} - \underset{\sim}{R})}$$

$$= \frac{2}{\pi} \sum_{\ell m} i^\ell\, Y_{\ell m}(\hat{r}) \int d^3s\, s^{-2}\, e^{-i\underset{\sim}{s}\cdot\underset{\sim}{R}}\, Y^*_{\ell m}(\hat{s}) j_\ell(sr) , \tag{2.16}$$

one obtains (see for instance Kocbach, 1976)

$$\int_{-\infty}^{\infty} dt\, e^{i\omega t} \langle \phi_f | Z_1 / |\underset{\sim}{r} - \underset{\sim}{R}_b(t)| | \phi_i \rangle = (-1)^{\ell_f - m_f} \delta_{\mu_f \mu_i}$$

$$\times \frac{2}{\pi} \sum_{\ell=0}^{\infty} i^{\ell} \langle \ell_f || Y_\ell || \ell_i \rangle \sum_{m=-\ell}^{\ell} \begin{pmatrix} \ell_f & \ell & \ell_i \\ -m_f & m & m_i \end{pmatrix} \int_0^{\infty} ds\, B_{\ell m}(q,b;s) F_\ell(s), \quad (2.17)$$

where

$$B_{\ell m}(q,b;s) = \int_{-\infty}^{\infty} dt\, e^{i\omega t} \int d\hat{s}\, Y^*_{\ell m}(\hat{s})\, e^{-i\underset{\sim}{s} \cdot \underset{\sim}{R}_b(t)}, \quad (2.18)$$

$$q \equiv \frac{\omega}{v_1} \geq E_B / \hbar v_1 \equiv q_0 \quad (2.19)$$

and

$$F_\ell(s) = \int_0^{\infty} dr\, r^2 j_\ell(sr) R^*_f(r) R_i(r), \quad (2.20)$$

where j_ℓ is the spherical Bessel function of order ℓ.

For a straight line projectile trajectory parallel with the z-axis in the xz-plane, Eq. (2.18) reduces to (Bang and Hansteen 1959, Kocbach 1976)

$$B_{\ell m}(q,b;s) = i^{\ell+m} \frac{\pi}{v_1 s} Y_{\ell m}(\cos^{-1}\frac{q}{s}, 0) \times J_m(b\sqrt{s^2 - q^2})\theta(s-q), \quad (2.21)$$

where J_m is the ordinary Bessel function of order m, and θ is the Heaviside function.

In the case of ionization, ϕ_f describes a one-electron continuum state ($\epsilon_f > 0$), and assuming ϕ_f to be normalized per unit energy, the ionization probability is given by

$$\frac{dI_b}{d\epsilon_f} = \sum_{\ell_f, m_f} |a_{fi}|^2 = \left(\frac{2Z_1 e^2}{mv}\right)^2 \sum_{\ell_f} \sum_{\ell, m} \frac{1}{2\ell+1} \times |\langle \ell_f || Y_\ell || \ell_i \rangle \int_0^{\infty} ds\, B_{\ell m}(q,b;s) F_\ell(s)|^2, \quad (2.22)$$

where we have summed over final state angular momentum. (Since we have

reinserted all the constants, this expression is independent of the system of units used.)

The corresponding total ionization probability I_b as a function of the impact parameter b, and the differential ionization cross section $d\sigma/d\epsilon_f$, may then finally be obtained by performing simple integrations over all final state continuum energies ϵ_f and over all impact parameters b, respectively.

3. Theory - configuration space formulation.

In the previous section we presented the SCA theory in its momentum space formulation, which - because it is readily generalized beyond the non-relativistic straight line path description of the projectile - has been the basis for our computer code. For a physical interpretation of the numerical results, however, the corresponding configuration space formulation may be equally illuminating.

In their original work on the SCA Bang and Hansteen (1959) showed that the straight line transition operator can be expressed as

$$\int_{-\infty}^{\infty} dt \; \frac{1}{|\underset{\sim}{r} - \underset{\sim}{R}_b(t)|} \; e^{i\omega t} = \frac{2}{v_1} K_0\left(q\sqrt{(x-b)^2 + y^2}\right) e^{iqz}, \qquad (3.1)$$

where K_0 is a MacDonald function (modified Bessel function of the third kind). This result is not very convenient, however, as it does not allow the use of angular momentum algebra in evaluating the matrix elements. What is needed is the multipole expansion of this expression. From the standard expansion

$$\frac{1}{|\underset{\sim}{r} - \underset{\sim}{R}_b(t)|} = \sum_{\ell,m} \frac{4\pi}{2\ell+1} \frac{r_<^\ell}{r_>^{\ell+1}} Y^*_{\ell m}(\hat{\underset{\sim}{R}}_b) \, Y_{\ell m}(\hat{\underset{\sim}{r}}) \qquad (3.2)$$

or, equivalently, by integrating Eq. (2.16) immediately over $\underset{\sim}{s}$, one finds the transition operator carrying quantum numbers (ℓ,m) to be (in a suitably chosen coordinate system),

$$I_{\ell m}(b,q;r) = \frac{1}{v_1}\sqrt{\frac{(2\ell+1)}{4\pi}\frac{(\ell-m)!}{(\ell+m)!}} \int_{-\infty}^{\infty} dT \; e^{iqT} \frac{r_<^\ell}{r_>^{\ell+1}} P_\ell^m\left(\frac{T}{\sqrt{b^2+T^2}}\right), \qquad m \geq 0 \qquad (3.3)$$

$$I_{\ell m}(b,q;r) = (-1)^m I_{\ell,-m}(b,q;r), \quad m < 0,$$

where $T = v_1 t$ and

$$r_> = \begin{cases} r, & r > \sqrt{b^2+T^2} \\ \sqrt{b^2+T^2}, & r < \sqrt{b^2+T^2} \end{cases} \qquad (3.4)$$

with a corresponding expression for $r_<$.

Inserting (3.4) into (3.3), we find that $I_{\ell m}(m \geq 0)$ can be written in the form

$$I_{\ell m}(b,q;r) = \frac{1}{v_1}\sqrt{\frac{(2\ell+1)}{4\pi}\frac{(\ell-m)!}{(\ell+m)!}}\left\{ r^{\ell}\bar{I}_{\ell m}(b,q) - \theta(r-b)\left[J^1_{\ell m}(b,q;r) - J^2_{\ell m}(b,q;r)\right]\right\}, \tag{3.5}$$

where

$$\bar{I}_{\ell m}(b,q) = \int_{-\infty}^{\infty} dT \frac{e^{iqT}}{(b^2+T^2)^{\frac{\ell+1}{2}}} P_\ell^m\left(\frac{T}{\sqrt{b^2+T^2}}\right) \tag{3.6}$$

is independent of r, while

$$J^1_{\ell m}(b,q;r) = \frac{1}{r^{\ell+1}} \int_{-\sqrt{r^2-b^2}}^{\sqrt{r^2-b^2}} dT\, e^{iqT}(b^2+T^2)^{\ell/2} P_\ell^m\left(\frac{T}{\sqrt{b^2+T^2}}\right), \tag{3.7}$$

and

$$J^2_{\ell m}(b,q;r) = r^{\ell} \int_{-\sqrt{r^2-b^2}}^{\sqrt{r^2-b^2}} dT \frac{e^{iqT}}{(b^2+T^2)^{\frac{\ell+1}{2}}} P_\ell^m\left(\frac{T}{\sqrt{b^2+T^2}}\right). \tag{3.8}$$

How the integrals $\bar{I}_{\ell m}$, $J^1_{\ell m}$ and $J^2_{\ell m}$ can be evaluated explicitly is outlined in the appendix.

From Eq. (3.5) one can draw some important qualitative conclusions. These are most clear in the $\ell = 0$ case, because in that case the orthogonality of the initial and final states will make the contribution from the first term of Eq. (3.5) vanish. Thus only the part of the wavefunctions outside $r = b$ contributes to the monopole amplitude. Furthermore, for large b, the rapid fall-off of the bound state wavefunction will make the contributing parts of the wavefunctions quite narrow.

For higher multipole transitions, which actually dominate at sufficiently large impact parameters, the situation is slightly more involved, because the

first term in Eq. (3.5) will dominate at large impact parameters. Thus it might look like this would make the transition amplitude far less dependent on the wavefunctions. However, at small b , $J^2_{\ell m}$ will effectively cancel $r^{\ell} I_{\ell m}$ thus again making the transition amplitude quite sensitive to the choice of wavefunctions.

Thus we arrive at the conclusion that when a straight line path is justified, the ionization probability is quite sensitive to the details of the wavefunctions outide the impact parameter. For distant collisions, i.e. impact parameters outside the radius of the target wavefunctions, the rapid fall-off of the wavefunction will make the transition amplitude strongly dependent on the electronic wavefunctions in a relatively narrow region just outside the impact parameter. Thus, the ionization probability in rapid collisions at large impact parameters gives information directly on the spatial distribution of the wavefunctions. This is in some sense complementary to the information obtained from slow collisions, which implies small impact parameters, in which case the ionization probability mostly reflects the high momentum tail of the momentum space wavefunction, as seen in the importance of the relativistic effects (for a review, see Amundsen 1978).

4. Numerical Methods.

The one-electron reduced radial Schrödinger equation was solved numerically using the Numerov integration method. For the bound states we used the logarithmic radial coordinate $\rho = \ln r$ with $\rho_{min} = -10$, and the integration was cut off when the reduced radial function $rR(r) \sim 10^{-5}$. This corresponds to $\Delta\rho$ being in the range 0.02-0.05 on a 256-point mesh. The one-electron bound state energies were determined with a relative error better than 1 ppm, and the relative error in the wavefunction should thus not exceed 10^{-3}. In fact, extensive tests on cases where the analytic solution was known, indicated that the accuracy was normally at least an order of magnitude better, and it can easily be improved if required.

Concerning the continuum solutions we distinguished between an interior region where we used the above logarithmic coordinate ρ, and an outer region where r itself was used as radial coordinate. The boundary between the two regions was chosen such that the number of mesh points in a wavelength always exceeded a certain minimum value (normally ~ 20). To determine the proper normalization, the last 10 to 20 maxima of the reduced radial wave were located by interpolation, and subsequently extrapolated to infinity. Again extensive tests on cases where the solution was known, indicated that the relative error in the normalization thus obtained was normally better than 10 ppm.

To calculate the spherical Bessel transforms, Eq.(2.20), we applied a technique devised by J.D. Talman (1978). We first interpolated the (now properly normalized) continuum function onto the same logarithmic radial mesh that was used for the bound-state function in question. This could be safely done because of the exponential cut-off introduced by the bound-state function which effectively limited the region of integration to the size of the target atom, or rather the appropriate shell. Taking a logarithmic mesh in momentum space as well, the resulting integral is

recognized as being a convolution and it can be performed by taking two successive fast Fourier transforms - no calculations of Bessel functions are thus required. The relative error introduced by the transform as such, and with $\rho_{min} = -10$, is generally better than 1 ppm, and the accuracy of the result is accordingly governed by the accuracy of the wavefunctions.

Concerning the straight-line path factor $B_{\ell m}$, Eq. (2.21), a three-term recursion scheme can be established from the well-known recursion relations obeyed by $Y_{\ell m}$ and J_m,

$$\bar{B}_{\ell m} = \bar{B}^*_{\ell m} \equiv i^{\ell - m} B_{\ell m}, \tag{4.1}$$

$$\bar{B}_{\ell+1,m} = \sqrt{\frac{(2\ell+1)(2\ell+3)}{(\ell+1+m)(\ell+1-m)}}\ \frac{q}{s}\bar{B}_{\ell m} - \sqrt{\frac{(2\ell+3)(\ell^2-m^2)}{(2\ell-1)[(\ell+1)^2-m^2]}}\ \bar{B}_{\ell-1,m}, \tag{4.2}$$

$$\bar{B}_{\ell+1,\ell+1} = -\sqrt{\frac{2\ell+3}{2\ell+2}}\ \frac{2\ell}{sb}\bar{B}_{\ell,\ell} - \sqrt{\frac{(2\ell+3)(2\ell+1)}{2\ell(2\ell+2)}}\ \frac{s^2-q^2}{s^2}\bar{B}_{\ell-1,\ell-1}. \tag{4.3}$$

To start off the recursion, B_{oo} and B_{11} were calculated directly from Eq(2.21), using appropriate series expansions for J_o and J_1 (Abramowitz and Stegun 1965). It should perhaps be noted that relation (4.3) becomes rather dangerous for small values of the argument of the Bessel function. This is not a serious problem, however, and it may be tackled simply by inverting the recursion scheme and recurring towards smaller values of ℓ and m. In the present work we chose instead to apply Eq. (2.21) directly in the critical cases, calculating J_m by means of series expansions. It was thoroughly checked that no serious accumulation of round-off errors

occurred during the remaining recursion, the relative error being of the order of 10^{-3} or better.

All numerical quadratures were performed using a fifth-order recursive relation. We feel confident that the overall accumulated relative error is in all cases less than 1% - probably closer to 0.1%, and it can be improved without much effort if required. The fact that in the straight line projectile trajectory case the total differential cross section $d\sigma/d\epsilon_f$ can be calculatec in two different ways (Bethe and Jackiw 1968),

$$\frac{d\sigma}{d\epsilon_f} = 2\pi \int_0^\infty db\, b \frac{dI_b}{d\epsilon_f}$$

$$= \frac{32\pi Z_1^2}{v_1^2} (2\ell_i + 1)(2\ell_f + 1) \sum_\ell \left| \begin{pmatrix} \ell_f & \ell & \ell_i \\ 0 & 0 & 0 \end{pmatrix} \right|^2 \int_q^\infty \frac{ds}{s^3} |F_\ell(s)|^2 \qquad (4.4)$$

where the last expression is identical to the standard PWBA-result, provides a further numerical check on our results.

5. Numerical results.

5a. Choice of one-electron orbitals.

From the discussion of section 2, it is clear that the SCA, like all other perturbative approaches, takes a particularly simple and easily interpreted form when the target electronic wavefunction is approximated by a single Slater determinant constructed from mutually orthogonal one-electron spin-orbitals. One should therefore examine more closely how well such an approach can actually work before one embarks on calculations with more elaborate wavefunctions incorporating configuration mixing and correlation.

In the present investigation we have employed one-electron wavefunctions supported by the variationally optimized effective central potentials (OPM) reported by Aashamar et al.(1978), and comparison is made with the corresponding results obtained with hydrogenic functions. The OPM potentials have been determined in such a way that the total energy of the target atomic state concerned, calculated with respect to the proper single-configuration determinantal approximation constructed from one-electron orbitals supported by the potential, is minimized with respect to variations in the potential. The resulting total energy is within a few ppm from the corresponding true single-configuration Hartree-Fock value (Aashamar et al. 1979), and the difference between corresponding one-electron orbitals is negligible. Insofar as the energy criterion is concerned, the OPM orbitals thus represent the optimum among the sets of orbitals that are derivable from single central potentials - the Herman-Skillman or Hartree-Fock-Slater orbitals included.

The theory as outlined in section 2 implicitly assumes that the ionized atom does not relax appreciably before the vacancy decays. This amounts to assuming that the effective potential is the same for the initial and final state, respectively. A check on the validity of

this assumption can be obtained by comparing the binding energy calculated according to Eq. (2.13) with experimental x-ray energies. In the cases focused on in the present paper, namely carbon and neon K-shell and argon L-shells, Eq. (2.13) predicts too strong binding by about 8, 3, and 5% respectively.

The discrepancy could probably be reduced substantially by separately optimizing the effective potential of the ion state. This would, however, seriously complicate the computational scheme by introducing sets of non-orthogonal orbitals in violation of one of the basic assumptions of the simple formulation in section 2. In purely hydrogenic calculations it has been common practice to use the experimental x-ray value for the binding energy instead of the value resulting from Eq. (2.13) - which incidentally should not be confused with the one-electron orbital eigenvalue. It can be argued that this is not an unreasonable device (Merzbacher and Lewis, 1958), but from the point of view of theoretical consistency it is obviously more satisfactory to use the value of E_B as determined by Eq. (2.13), and the more so the more elaborate the wavefunctions are. It is well known that a moderate change in the value of E_B while the wavefunctions are kept fixed can produce large effects in the corresponding ionization cross sections. This is particularly the case for slow collisions, where it can also fairly readily be demonstrated analytically. In very slow collisions the cross section for ionization to a particular final state falls off like

$$\frac{d\sigma}{d\epsilon_f} \propto \frac{1}{E_1} q^{-2(4+\ell_i+\ell_f)}, \quad q \to \infty \tag{5.1}$$

(or faster, due to possible cancellations) in a non-relativistic electron description (cf. Amundsen 1977). The result follows from the fact that the product of the radial wavefunctions behaves like $r^{\ell_i+\ell_f}$ at small r, which together with Eq. (2.20) leads to

$$F_\ell(s) \propto s^{-(3+\ell_f+\ell_i)}, \quad s \to \infty \tag{5.2}$$

independent of the details of the wavefunctions and of ℓ. Using Eq.(4.4) one immediately arrives at the result (5.1).

Obviously, a change of E_B away from the theoretically consistent value of Eq. (2.13), will thus produce a pronounced effect in the low projectile energy behaviour of the cross section, and is therefore from a theoretical point of view somewhat ambiguous since it may tend to obscure the effect of improving the wavefunctions as such in this collision energy range.

In the present paper we have used Eq.(2.13) in all calculations except for the carbon K-shell where we used the experimental x-ray binding energy. The significance of the difference will be discussed in more detail below. In all cases where we compare with hydrogenic calculations, the same binding energy is used for both sets of wavefunctions, allowing us to claim that the differences are pure wavefunction effects.

5b. K-shell ionization.

We have carried out systematic calculations on proton-induced K-shell ionization of Ne and C in the collision energy range 0.1-10 MeV, sufficiently supplemented by calculations for other elements and energies to establis general trends. Our hydrogenic results agree with the tabulated values of Hansteen et al. (1975) within 10% or better, which is consistent with earlier experience for lower scaled energies (larger $q_o a_K$, Amundsen 1976).

Figs. 2a-h show the ionization probability for Ne for E_1 = 0.1-10 MeV. It is evident from the figures that the wavefunction effects are important except when $q_o^{-1} \sim 1.4\text{-}1.8\ a_K$ ($q_o^{-2} \sim 2\text{-}3\ a_K^2$), where the difference is observed to be very small. For higher energies ($q_o^{-1} \gtrsim 2a_K$) the details of the wavefunctions become quite important, and what is more significant, the effect is strongly b-dependent. The large increase when the impact parameter

becomes comparable with the L-shell radius supports the conclusion of section 3 that for large b in fast collisions L_b should reflect the spatial distribution of the wavefunctions. It is also consistent with the idea behind the outer screening prescription normally applied in the PWBA (Merzbacher and Lewis 1958). Our OPM results for total cross sections indeed agree to within 10-15% with the tabulated PWBA values of Khandelwal et al. (1969), lying in general slightly below.

At low energies the wavefunction effects give rise to a reduction of the ionization probability, a reduction which increases with b. This general trend was also found by Aashamar and Kocbach (1976), but the overall importance of the wavefunction effects appears to be somewhat larger than these authors, and also Pauli et al. (1978), report. This may simply be ascribed to the fact that Herman-Skillman potentials (1963) were used in their calculations.

Figs. 3a-d illustrate the angular momentum distribution of the wavefunction effects in a typical case (3 MeV protons on Ne). In agreement with the results of section 3, the sensitivity of the multipole amplitudes to the choice of wavefunctions is seen to decrease with increasing value of ℓ. The total ionization probability is largely determined by the monopole and dipole transitions at small b, and by dipole transitions at large b. In fact, as can be seen from Eq. (3.1), the ionization amplitude at small q and large b becomes roughly proportional to the photoionization amplitude (in the dipole approximation). The importance of the wavefunction effects should thus roughly show the same picture as in photoionization calculations. However, for all cases where the non-relativistic projectile description can be employed, one has $q_0 >> \Delta E/c$ (ΔE being the energy transfer), and accordingly the deviation from the dipole approximation will never be negligible, and will to some extent reduce the wavefunction effects.

This can be seen to be the case in the example shown in Figs. 3. The qualitative features of the neon results remain valid for all systems examined, when properly scaled, and the importance of the effects increases with decreasing target nuclear charge Z_2, as might be expected. In Figs. 4a-d we show our results for protons on carbon. For this rather symmetric system the use of perturbation theory may of course be questionable for the collision energies considered here ($E_1 \approx 200$-600 keV), since the projectile velocity is comparable to the target K-shell velocity. But this should not affect the importance of the wavefunction effects. For the higher energies the figures show a substantial improvement in the agreement between theory and experiment upon using improved wavefunctions. For 200 and 300 keV the effect is rather small. Concerning 200 keV there also appears to be a discrepancy between the two sets of experimental data available, which have been obtained by two different methods. The data of Horsdal Pedersen et al. (1979) were derived from measurements on Auger electrons from a CH_4 target, whereas the data of Weber and Bell (1977) come from x-ray measurements on a carbon foil. Although one can list several reasons why the two sets of measurements may not be entirely compatible, it is difficult to see what mechanism would make the difference as strongly dependent on impact parameter as seems to be the case. Weber and Bell (1977) also report results for 100 and 150 keV projectile energy, respectively, but in these cases the hydrogenic as well as the improved wavefunctions give values consistent with the experiments (without any attempt to correct for higher order effects).

Fig. 4d also illustrates the effect of replacing the consistent binding energy according to Eq. (2.13) by the experimental x-ray energy. The case shown is the one among those reported where the effect is most pronounced, as well as the one where the discrepancy between theory and experiment is most evident.

It seems reasonable to assume that the improvement one may expect from refining the description of initial and final states to the point where

the x-ray energy is reproduced within the experimental error, is typically of the same order of magnitude as the change resulting from simply inserting the experimental binding energy into the calculation with no corresponding change in the wavefunctions. Obviously, however, the lack of ability of the initial and final state total wavefunctions to reproduce accurately the experimental x-ray energies may be taken as an indication of corresponding errors in other matrix elements involved as well. The effect of the inaccuracy in E_B is accordingly not easily disentangled from the effect of the accompanying error in the wavefunctions. It is for instance not generally clear under what circumstances the two effects will pull in the same direction, and when they will tend to partly cancel each other. In the present case of the OPM wavefunctions the uncertainty both in E_B and in the wavefunctions obviously derives mostly from the final state which has not been made subject to any optimization whatsoever. The problems invoked in trying to separately optimize the final state description have already been touched upon in subsection 5a. One might contemplate a multi-configuration approach to improve the quality of the wavefunctions, but even then one would face the question of relaxation and how to avoid introducing non-orthogonal sets of one-electron orbitals. These problems are essentially the same as those encountered in photoionization (see for example Pratt et al. 1973). Although a more sophisticated calculation along these lines may not improve significantly the agreement between theory and experiment, it would nevertheless be of value in the way of establishing the limits of performance of the present simple model. Also, one should not forget the possible importance of effects arising from terms beyond first order in perturbation theory (see for example Basbas et al. 1973, 1978, Ford et al. 1977). Finally, the fact that for instance the carbon target is not a monoatomic gas, may modify the wavefunctions, in particular in the continuum, to a significant extent.

5c. L-shell ionization.

We have not attempted to perform a comprehensive set of calculations for the L-shells, because experimental L-shell ionization probabilities as functions of b are only available for heavy systems where electronic relativistic effects and Coulomb deflection should also be included (Amundsen 1977), and that is outside the scope of the present paper. In general our hydrogenic calculations confirm the tabulated values of Hansteen et al. (1975) to within 15% (poorest agreement at high energies). The total cross-sections obtained using OPM wavefunctions also apparently agree within 10% with the PWBA calculations of Manson (1972) and Choi (1975) based on Herman-Skillman wavefunctions. The discrepancies are probably entirely due to the different choices of wavefunctions and binding energies. Furthermore, our OPM calculations also reproduce the characteristic shape of the δ-electron spectrum at very low E_f (Manson 1972).

Figs 5a-d show our results for I_b for the L_1 and $L_{2,3}$ shells of argon at 0.1 and 1 MeV collision energy, respectively. The wavefunction effects are, as expected, much larger than for K-shell ionization, and they also show a much more complicated impact parameter dependence.

Concerning the L_1-shell (Figs. 5a,b) one notes that the characteristic dip in the b-distribution due to the node in the 2s radial wavefunction (Hansteen et al. 1974) is extremely sensitive to the choice of wavefunctions, as the dip appears only at 0.1 MeV for the hydrogenic wavefunctions and only at 1 MeV in the case of the OPM wavefunctions.

In the case of the $L_{2,3}$-shells there is of course no dip reflecting wavefunctions effects, but apart from that the dependence on the details of the wavefunctions is even more pronounced. This is consistent with the well-known fact that the $\ell_i = 1$ (and higher) wavefunctions are much more sensitive to the details of the effective potentials than the s-functions.

6. Conclusions.

Our results show that the wavefunction effects are in general quite large and strongly impact parameter dependent for light systems. The magnitude of the effects increases as one goes to higher atomic shells, but decreases for higher multipole contributions. A characteristic feature seems to be that at low collision energies the wavefunction effects tend to reduce the ionization probability as compared with the hydrogenic results, whereas at higher energies we find a substantial increase. In between, for collisions where the projectile velocity is comparable or slightly lower than the initial velocity of the ejected electron, there is a narrow range where the ionization mechanism does not discriminate appreciably between different wavefunctions. These features are substantiated by available experimental data on carbon and neon K-shell ionization, where the use of the OPM wavefunctions improves the agreement between theory and recent experiments, especially for the more rapid collisions.

It is also shown that at large impact parameters the SCA transition operator is determined mainly by the atomic wavefunctions in a relatively narrow region around the impact parameter. For such collisions the ionization probability thus reflects the spatial distribution of the wavefunctions rather directly, which is in accordance with the numerical calculations.

The remaining discrepancies between theory and experiment may probably be somewhat reduced by further improvement of the atomic final state description, but it is also reasonable to assume that they partly reflect the inadequacy of the first-order theory.

Acknowledgements.

We are greatly indepted to E. Horsdal Pedersen, F. Folkmann and N.H. Pedersen in the Aarhus group for making their experimental results available to us prior to publication. We would also like to express our appreciation of many enlightening discussions with E. Horsdal Pedersen and D.H. Jakubassa. One of the authors (K.Aa.) wishes to acknowledge the partial support by the Norwegian Research Council for Science and the Humanities.

Appendix

In this appendix we evaluate the integrals 3.6-3.8.

Writing $R = \sqrt{b^2 + T^2}$, we note that from the recursion relations of the associated Legendre functions we have (for $0 \leq m < \ell$)

$$P_\ell^m (T/R)/R^{\ell+1} = \frac{-1}{\ell - m} \frac{d}{dT} \left(P_{\ell-1}^m (T/R)/R^\ell \right). \tag{A.1}$$

By partial integration in Eq.(3.6) we thus derive

$$\bar{I}_{\ell m}(b,q) = \frac{iq}{\ell - m} \bar{I}_{\ell-1,m}(b,q) . \tag{A.2}$$

Consequently we need only evaluate $\bar{I}_{\ell\ell}$. Since

$$P_\ell^\ell(T/R) = \frac{(-1)^\ell (2\ell - 1)!! b^\ell}{(b^2 + T^2)^{\ell/2}} , \tag{A.3}$$

we find immediately from Basset's formula (Abramowitz and Stegun 1965, Eq. 9.6.25),

$$\begin{aligned} \bar{I}_{\ell\ell} &= 2(-1)^\ell (2\ell - 1)!! b^\ell \int_0^\infty \frac{\cos(qT)}{(b^2 + T^2)^{\ell+\frac{1}{2}}} \\ &= 2(-1)^\ell q^\ell K_\ell(bq), \end{aligned} \tag{A.4}$$

and thus, from (A.2):

$$\bar{I}_{\ell m} = \frac{2i^{\ell+m}}{(\ell-m)!} q^\ell K_m(bq). \tag{A.5}$$

The relation (A.1) can likewise be used to reduce $J^2_{\ell m}$ by partial integration for $0 \leq m < \ell$,

$$\begin{aligned} J^2_{\ell m}(b,q;r) = &- \frac{e^{iqT}}{(\ell-m)} \left(\frac{r}{R}\right)^\ell P_{\ell-1}^m (T/R) \Big|_{-\sqrt{r^2 - b^2}}^{\sqrt{r^2 - b^2}} \\ &+ \frac{iqr}{\ell-m} J^2_{\ell-1,m}(b,q;r) \end{aligned} \tag{A.6}$$

Again we only need to evaluate the integral explicitly for $\ell = m$. To do this we need the following generalization of Basset's formula

$$J^2_{\ell\ell}(b,q;r) = 2(-1)^\ell (2\ell-1)!!(br)^\ell \int_0^{\sqrt{r^2-b^2}} dT \frac{\cos(qT)}{(b^2+T^2)^{\ell+\frac{1}{2}}}$$

$$= 2(2\ell-1)!!\left(\frac{r}{b}\right)^\ell \mathrm{Re} \int_{i\pi/2}^{\sinh^{-1}\left(\sqrt{\left(\frac{r}{b}\right)^2-1}\right)+i\pi/2} dw \frac{e^{-bq\cosh w}}{(\sinh w)^{2\ell}} \qquad (A.7)$$

$$= 2(-1)^\ell (qr)^\ell \mathrm{Re}\left[K_{-\ell}\left(\sinh^{-1}\left(\sqrt{\left(\frac{r}{b}\right)^2-1}\right)+i\pi/2,\ bq\right) - K_{-\ell}\left(\frac{i\pi}{2},\ bq\right)\right],$$

where we have put $T = ib\cosh w$ and used an integral representation of the incomplete MacDonald function of the Poisson form, $K_\nu(a,x)$, given by Agrest and Maksimov (1971, Eq. II.1.30). Actually they quote the result only for $\mathrm{Re}\,\nu \geq -1/2$, but as long as the path of integration in the w-plane does not cross or encircle $w = 0$, the integral in (A.7) is an analytic function of ℓ. Alternatively, the result may be established from the cited result for $\ell = 0$ by exploiting the recursion relations given in section II.2 in the book by Agrest and Maksimov (1971). Incidentally, $\mathrm{Re}K_{-\ell}\left(\frac{i\pi}{2},x\right) = 0$ as follows from Eqs. II.1.5, 13, 14, 17 and 18 of this reference.

Thus, iterating Eq. (A.6) and using Eq. (A.7), one readily obtains,

$$J^2_{\ell m}(b,q;r) = \sum_{\mu=1}^{\ell-m} i^{\mu+1}(qr)^{\mu-1}\left[e^{iq\sqrt{r^2-b^2}} + (-1)^{\ell-m-\mu+1} e^{-iq\sqrt{r^2-b^2}}\right]$$

$$\times \frac{(\ell-m-\mu)!}{(\ell-m)!} P^m_{\ell-\mu}\left(\sqrt{1-\left(\frac{b}{r}\right)^2}\right) \qquad (A.8)$$

$$+ 2\frac{i^{\ell+m}}{(\ell-m)!}(qr)^\ell \mathrm{Re}\, K_{-m}\left(\sinh^{-1}\left(\sqrt{1-\left(\frac{b}{r}\right)^2}\right)+\frac{i\pi}{2},\ bq\right).$$

Finally, $J^1_{\ell m}$ is elementary, but we give the expression for the sake of completeness. Analogously to (A.1), one has $(0 \leq m < \ell)$,

$$\frac{d}{dT}\left[R^\ell P^m_\ell (T/R)\right] = (\ell+m) R^{\ell-1} P^m_{\ell-1}(T/R) \qquad (A.9)$$

which gives

$$J^1_{\ell m}(b,q;r) = \frac{-i}{qr} e^{iqT} P^m_\ell\left(\frac{T}{R}\right) \Bigg|_{-\sqrt{r^2-b^2}}^{\sqrt{r^2-b^2}} - (\ell+m)\, J^1_{\ell-1,m}(b,q;r) \tag{A.10}$$

and again we only need the $\ell = m$ integral, which is (compare Eq. (A.3))

$$J^1_{\ell\ell}(b,q;r) = 2(-1)^\ell \frac{(2\ell-1)!!\, b^\ell}{r^{\ell+1}} \int_0^{\sqrt{r^2-b^2}} \cos(qT)\, = \frac{2\sin\left(q\sqrt{r^2-b^2}\right)}{qr} P^\ell_\ell\left(\sqrt{1-\left(\frac{b}{r}\right)^2}\right) \tag{A.11}$$

and thus, from (A.10)

$$J^1_{\ell m} = \sum_{\mu=0}^{\ell-m} \frac{i^{\mu-1}}{(qr)^{\mu+1}} \left[e^{iq\sqrt{r^2-b^2}} - (-1)^{\ell+m-\mu} e^{-iq\sqrt{r^2-b^2}} \right] \times \frac{(\ell+m)!}{(\ell+m-\mu)!} P^m_{\ell-\mu}\left(\sqrt{1-\left(\frac{b}{r}\right)^2}\right). \tag{A.12}$$

Figure captions.

Fig. 1. Classical picture of the collision between a charged particle moving along a trajectory $\underset{\sim}{R}_b(t)$ and an atomic system.

Fig. 2. The K-shell ionization probability I_b as a function of the impact parameter b for protons on neon. Proton energies: E_1 = 0.1 MeV (a), 0.5 MeV (b), 0.7 MeV (c), 1 MeV (d), 1.5 MeV (e), 2 MeV (f), 5 MeV (g), 10 MeV (h). Solid curves: Results obtained using OPM wavefunctions and consistent binding energy from Eq. (2.13). Dashed curves: Results corresponding to hydrogenic wavefunctions and OPM binding energy. Dash-dot curves (right-hand scale): Ratio r of OPM to hydrogenic results. The experimental values in cases (b), (c), (d), (e) are those of Horsdal Pedersen et al. (1979).

Fig. 3. The monopole contribution (a), dipole contribution (b), and quadrupole contribution (c) to the total K-shell ionization probability I_b (d) as functions of the impact parameter b for 3 MeV protons on neon. Otherwise same as Fig. 2.

Fig. 4. The K-shell ionization probability I_b as a function of the impact parameter b for protons on carbon. Proton energies: E_1 = 0.2 MeV (a), 0.3 MeV (b), 0.4 MeV (c), 0.6 MeV (d). Solid curves: Results obtained using OPM wavefunctions and experimental (x-ray) binding energy E_B. Dashed curves: Results corresponding to Slater-screened hydrogenic wavefunctions and experimental (x-ray) E_B. Dotted curve: Same as solid curves but with OPM binding energy from Eq. (2.13). The experimental results are those of Weber and Bell (1977) (⏃) and Horsdal Pedersen et al. (1979) (⏄).

Fig. 5. The L_1-shell (a,b) and $L_{2,3}$-shell (c,d) ionization probabilities I_b as functions of the impact parameter b for protons on argon. Proton energies: E_1 = 0.1 MeV (a,c), 1 MeV (b,d). Otherwise as in Fig.2. (Slater-screened wavefunctions were used in the hydrogenic cases.)

References.

Aashamar, O. and Kocbach, L., 1977, J. Phys. B: Atom. molec. Phys. 10, 869-78.

Aashamar, K., Luke, T.M., and Talman, J.D., 1978, At. Data and Nucl. Data Tables 22, 443-472.

Aashamar, K., Luke, T.M., and Talman, J.D., 1979, Phys. Rev. A19, 6-16.

Abramowitz, M. and Stegun, I.A., 1965, "Handbook of Mathematical Functions" (Dover, New York).

Agrest, M.M. and Maksimov, M.S., 1971, "Theory of Incomplete Cylindrical Functions and their Applications" (Springer, Berlin).

Amundsen, P.A., 1976, J. Phys. B: Atom. molec. Phys. 9, 971-83.

Amundsen, P.A., 1977, J. Phys. B: Atom. molec. Phys.10, 1097-1112.

Amundsen, P.A., 1978, "Notes from the Nordic Spring Symposium on Atomic Inner Shell Phenomena", Geilo, vol. II, eds. J.M. Hansteen and R. Gundersen (Bergen Univ., Dept. of Physics), 43-64.

Arthurs, A.M., 1959, Proc. Phys. Soc. 73, 681-4.

Bang, J. and Hansteen, J.M., 1959, K. Danske Vidensk. Selsk., Mat. - Fys. Meddr. 31, No. 13, 1-43.

Basbas, G., Brandt, W., and Laubert, R., 1973, Phys. Rev. A7, 983-1001.

Basbas, G., Brandt, W., and Laubert, R., 1978, Phys. Rev. A17, 1655-74.

Bauer, K.G., Fazly, Q., Mo.msen, H., Schürkes, P., and Pauli, M., 1978, Phys. Lett. 68A, 223-5.

Bethe, H.A. and Jackiw, R.W., 1968,
"Intermediate Quantum Mechanics", 2.ed.
(Benjamin, New York), 326-29.

Bohr, N., 1948, K. Danske Vidensk. Selsk.,
Mat. - Fys. Meddr. 18, No. 8, 1-21.

Choi, B.H., 1975, Phys. Rev. A11, 2004-10.

Ford, A.L., Fitchard, E., and Reading, J.F., 1977, Phys. Rev. A16, 133-9.

Hansteen, J.M., Johnsen, O.M., and Kocbach, L., 1974,
J. Phys. B: Atom. molec. Phys. 7, L 271-4.

Hansteen, J.M., Johnsen, O.M., and Kocbach, L., 1975,
At. Data and Nucl. Data Tables 15, 305-17.

Horsdal Pedersen, E., Folkmann, F., and Pedersen, N.H., 1979,
Univ. of Aarhus preprint, and private communication.

Khandelwal, G.S., Choi, B.H., and Merzbacher, E., 1969,
Atomic Data 1, 103-19.

Kocbach, L., 1976, Z. Phys. A279, 233-6.

Lægsgaard, E., Andersen, J.U., and Lund, M., 1978,
"Electronic and Atomic Collisions",
ed. G. Watel (North Holland, Amsterdam), 353-72.

Manson, S.T., 1972, Phys. Rev. A6, 1013-24.

Merzbacher, E. and Lewis, H.W., 1958,
Handb. Phys. 34 (Springer, Berlin), 166-92.

Pauli, M., Rösel, F., and Trautmann, D., 1978,
Phys. Lett. 67A, 28-30.

Pratt, R.H., Ron, A., and Tseng, H.K., 1973,
Rev. Mod. Phys. 45, 273-325 and 663-4.

Talman, J.D., 1978, J. Comp. Phys. 29, 35-48.

Weber, K.H. and Bell, [illegible], 1977, Phys. Rev. A16, 1075-81.

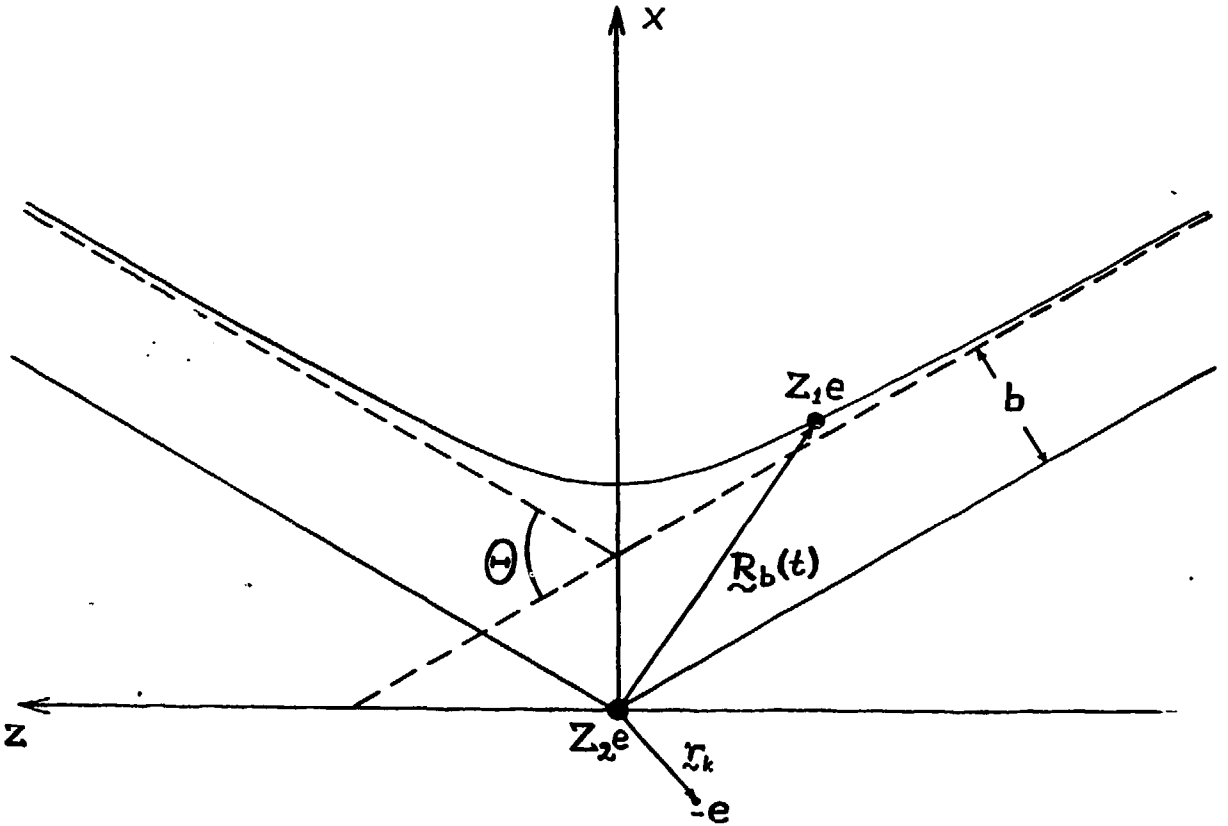

Fig. 1.

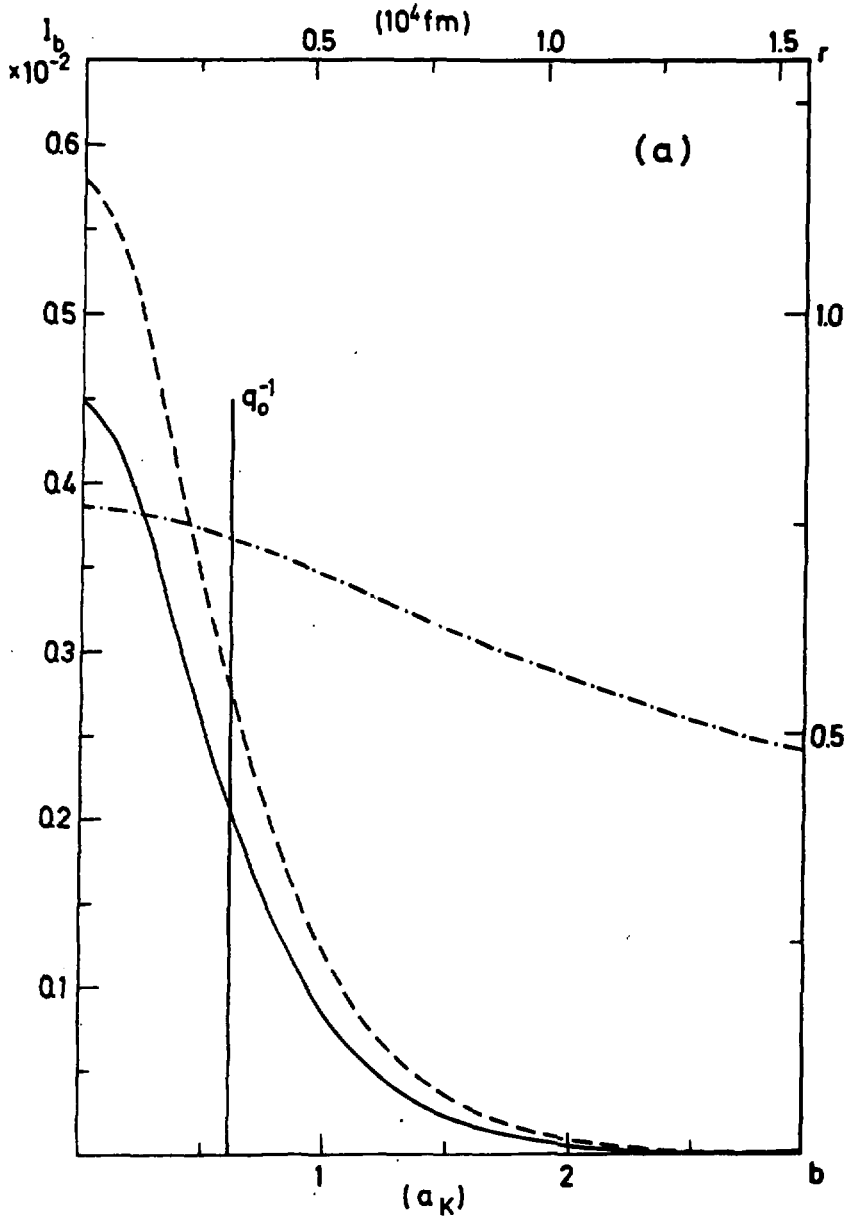

Fig. 2a.

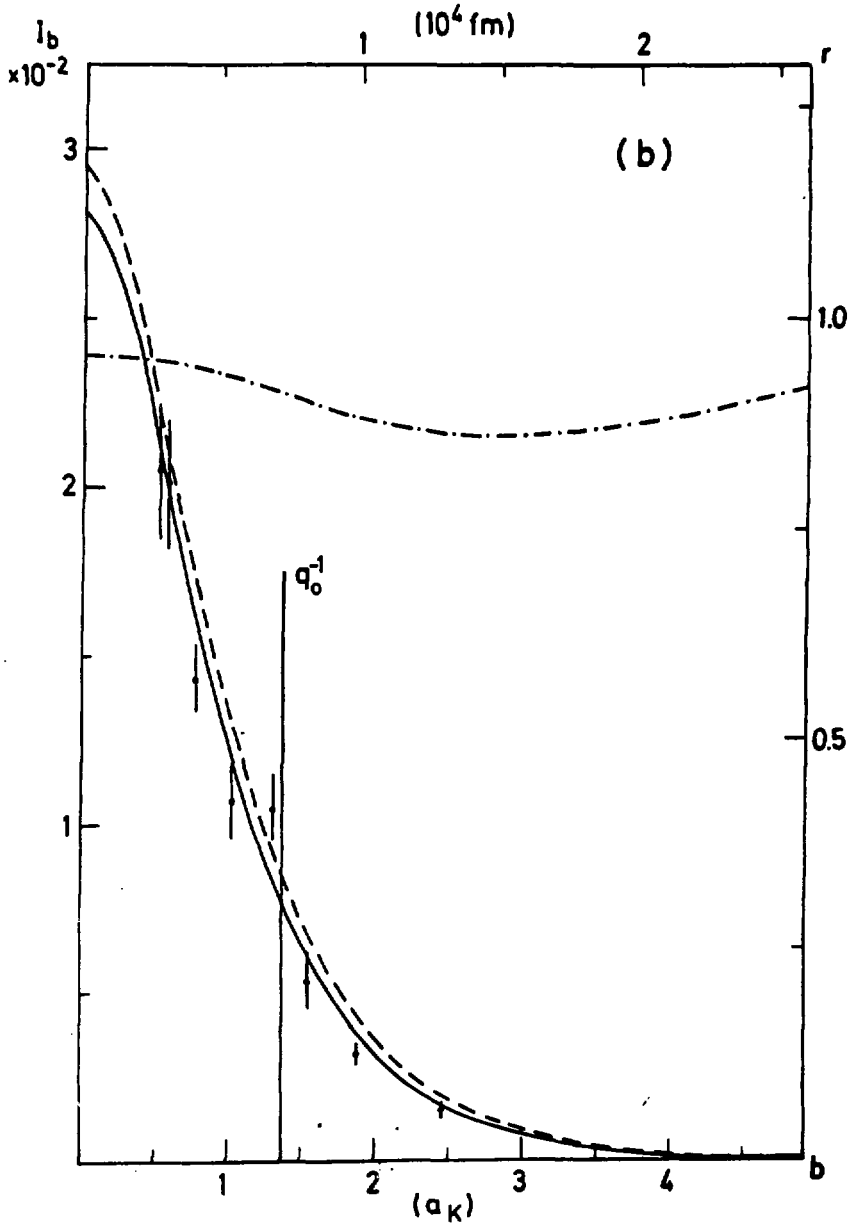

Fig. 2b.

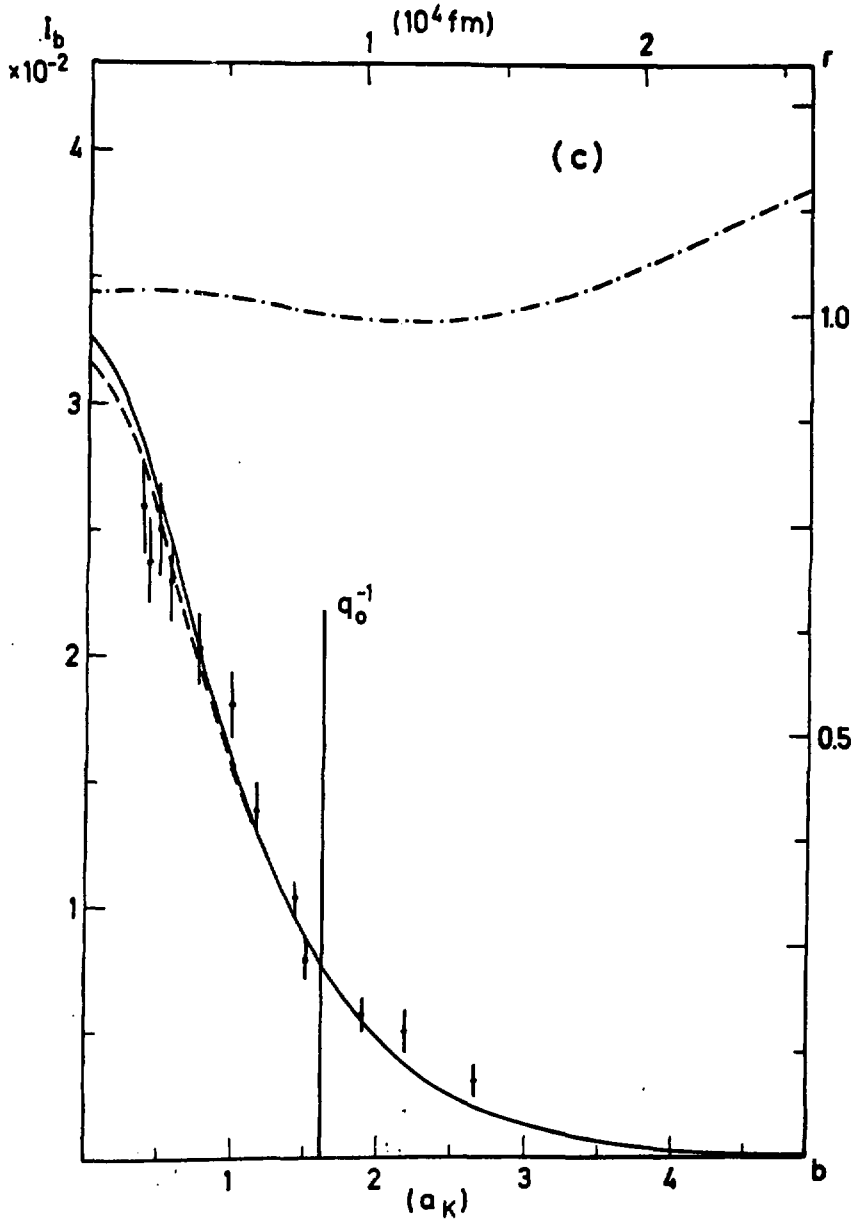

Fig. 2c.

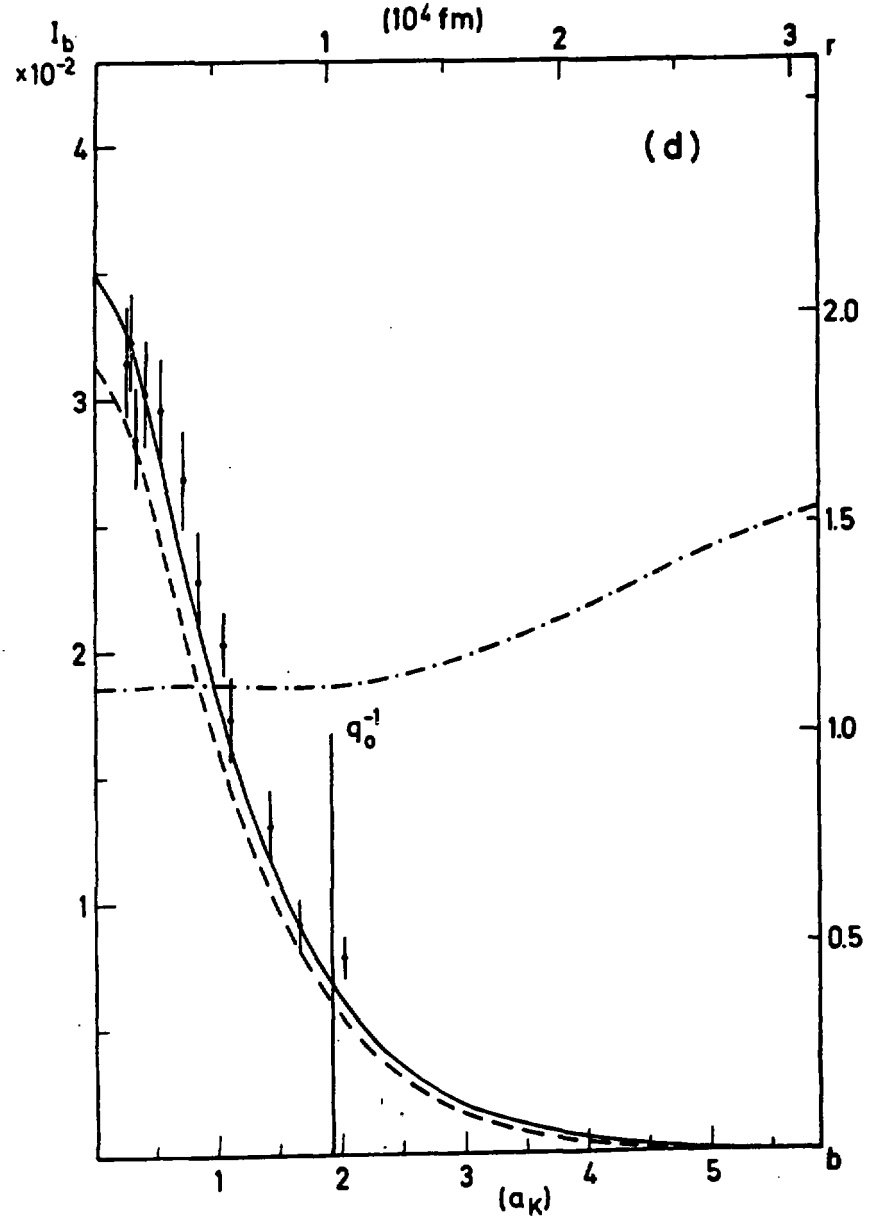

Fig. 2d.

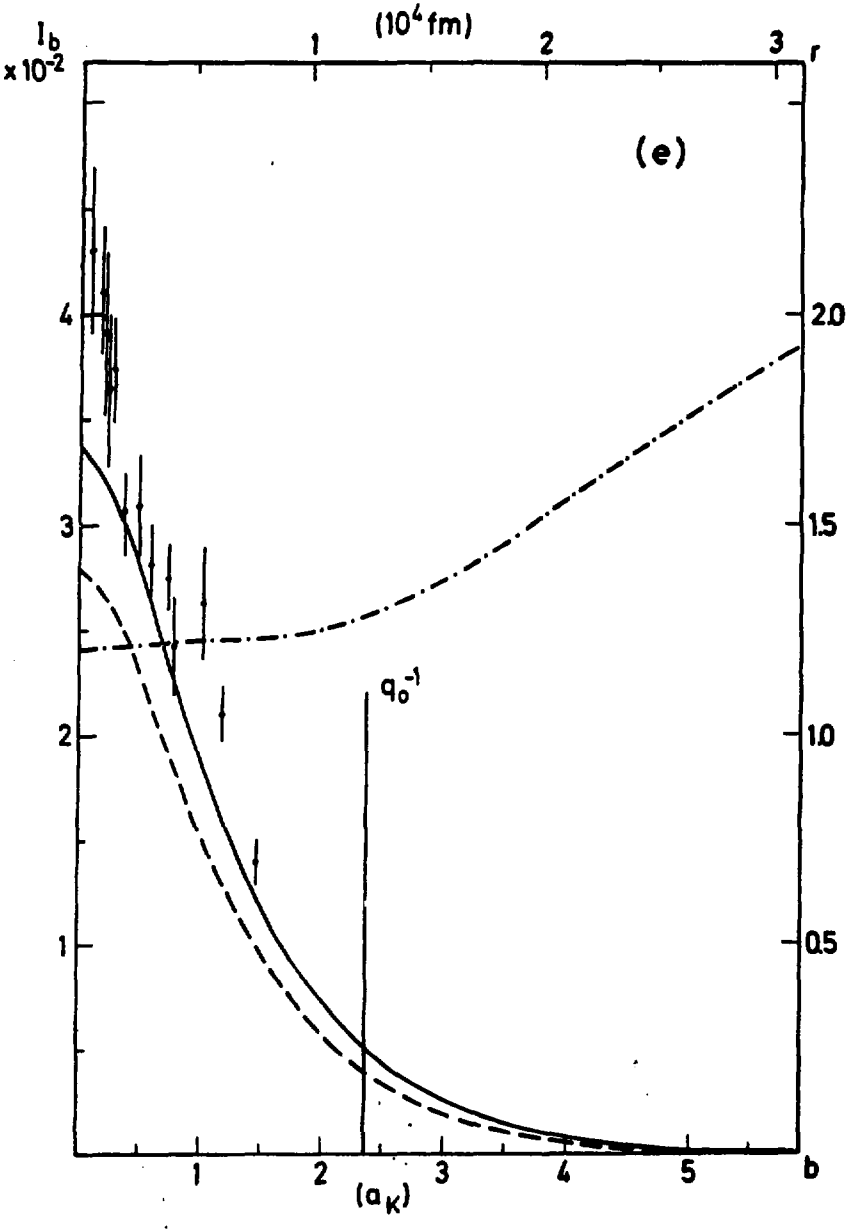

Fig. 2e.

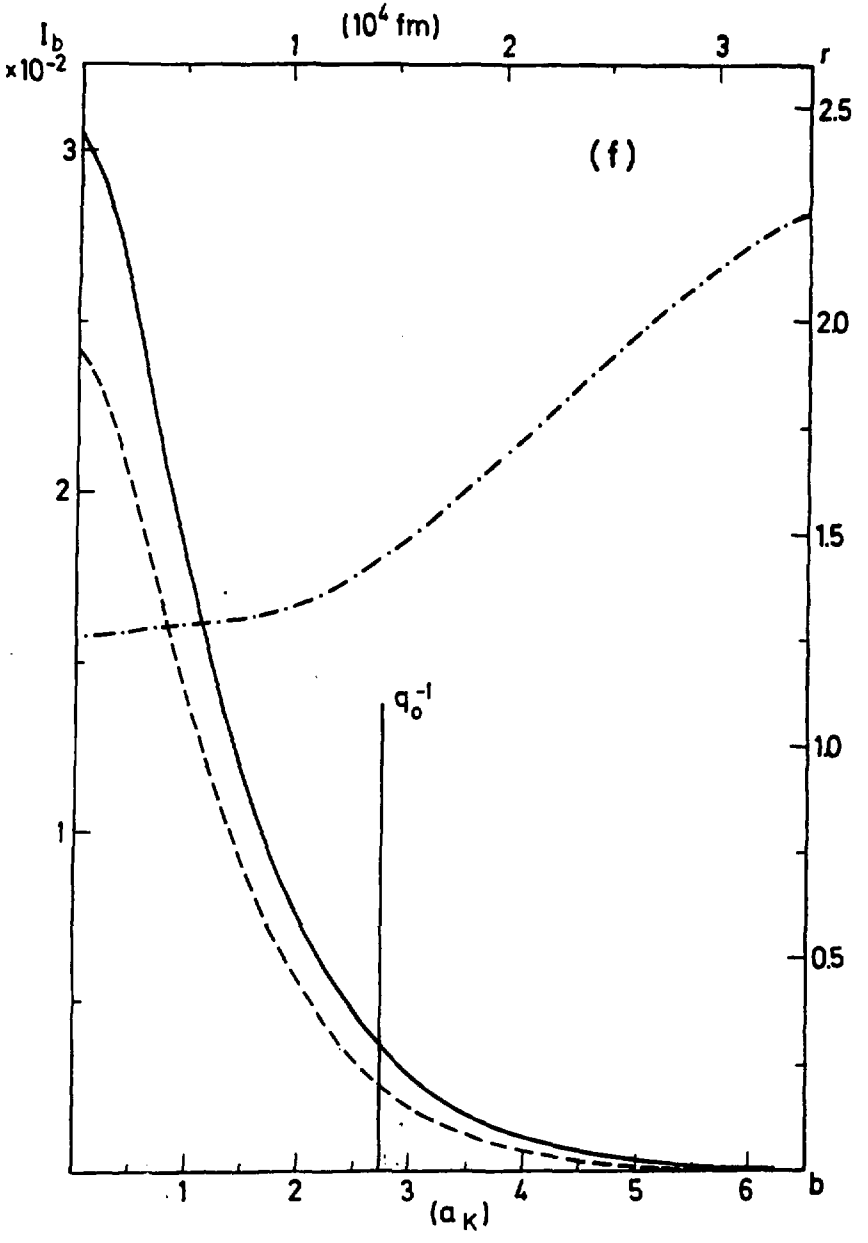

Fig. 2f.

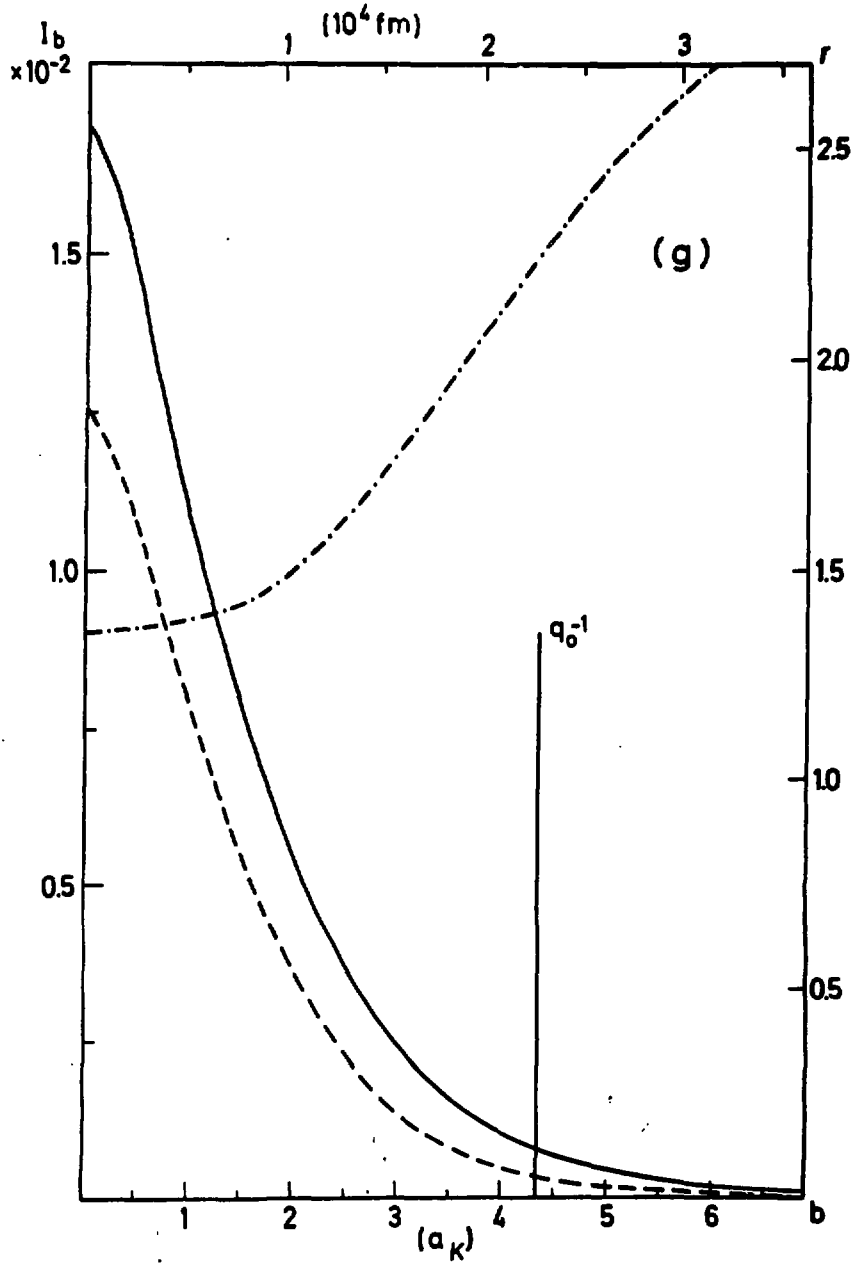

Fig. 2g.

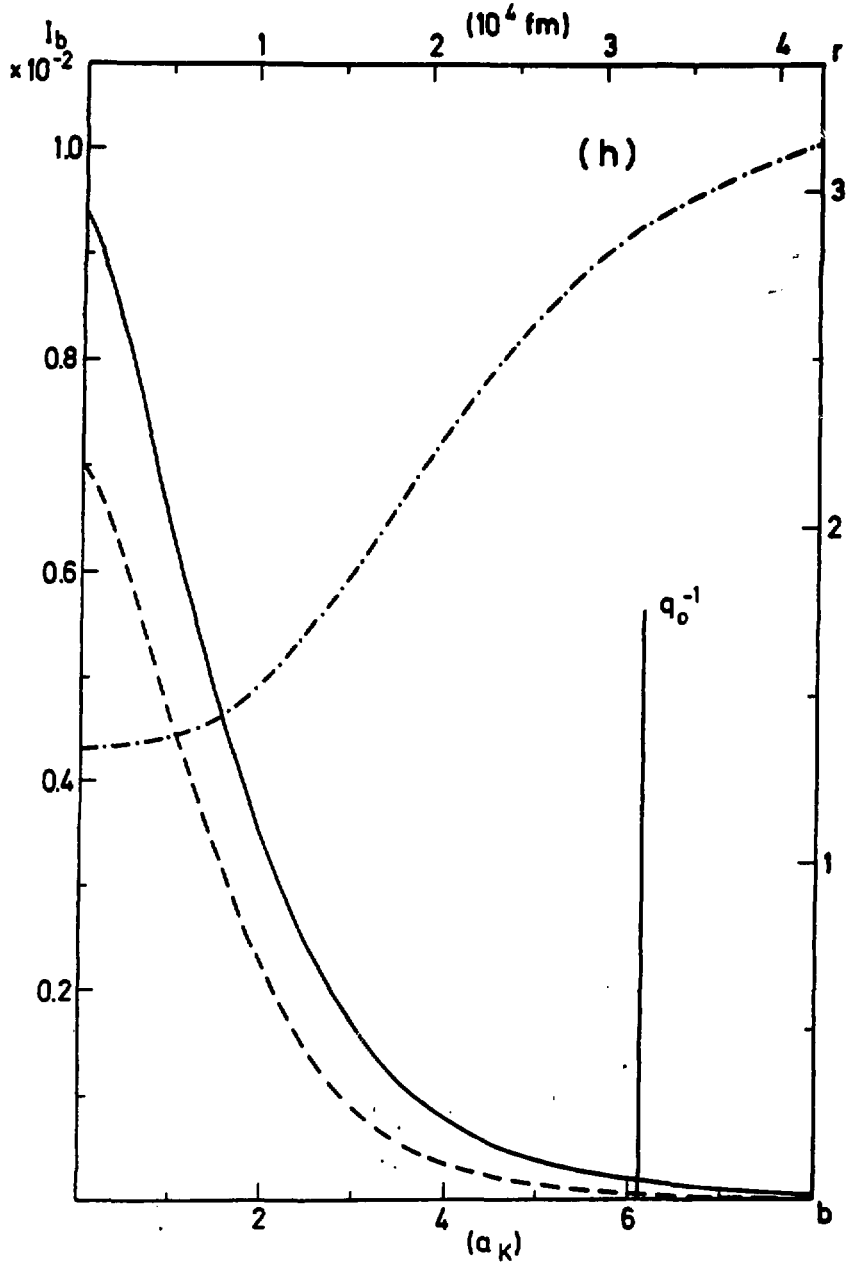

Fig. 2h.

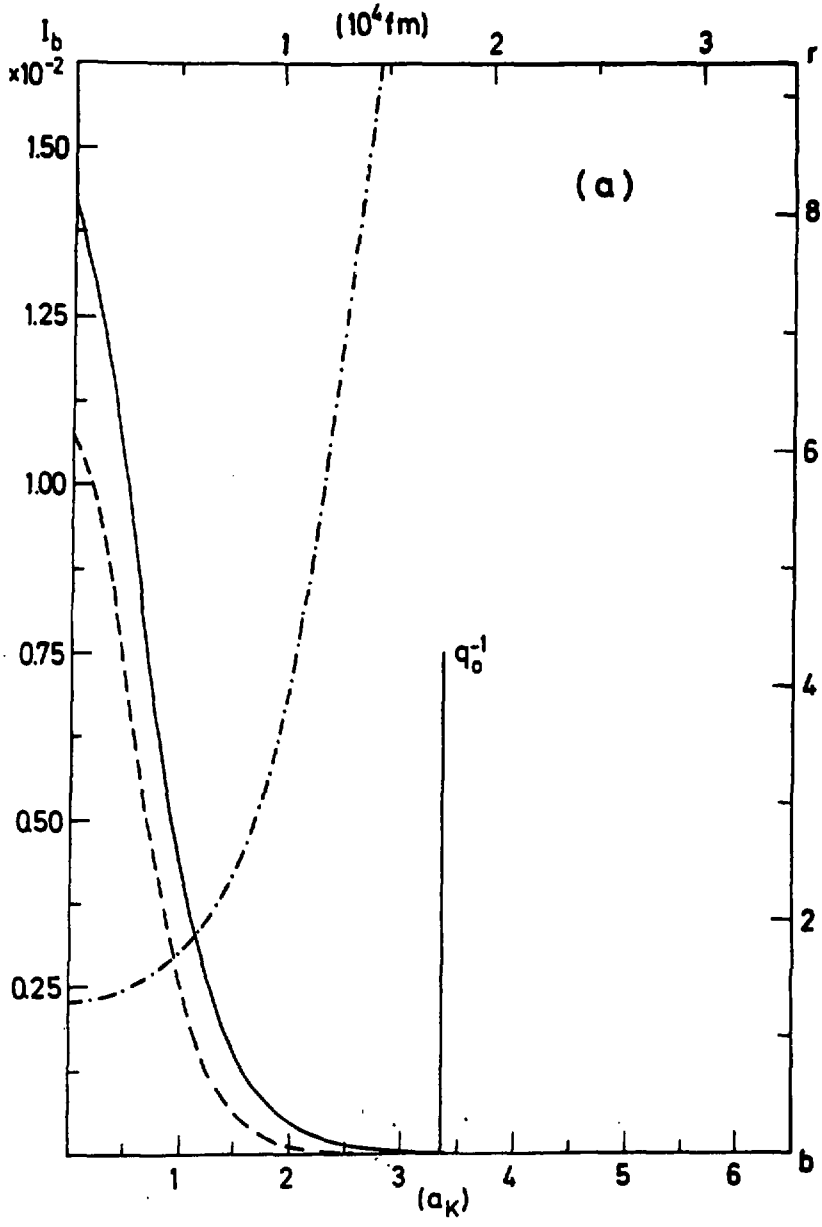
I_b
$\times 10^{-2}$
1.50
1.25
1.00
0.75
0.50
0.25
(10⁴ fm)
1
2
3
r
8
6
4
2
b
(a)
q_0^{-1}
1
2
3
4
5
6
(a_K)

Fig. 3a.

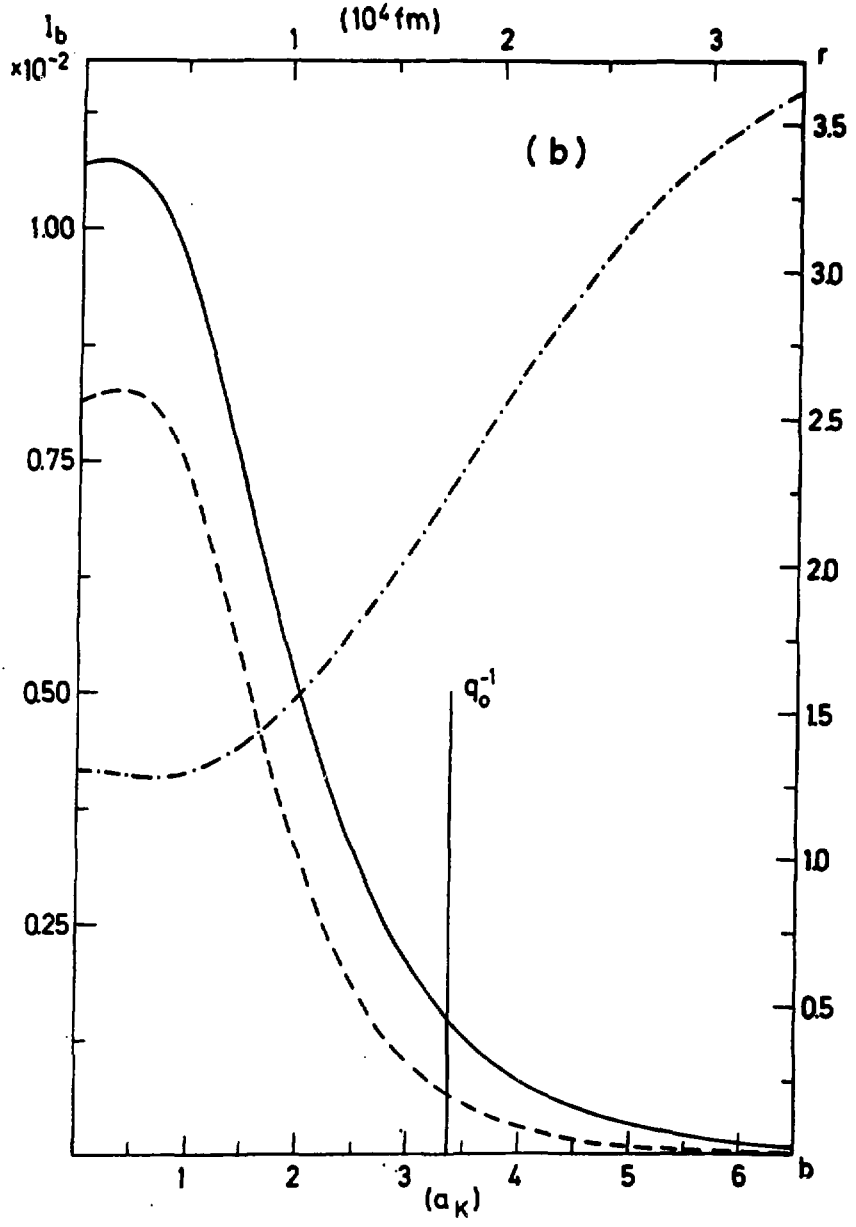
I_b
$\times 10^{-2}$
(10⁴ fm)
1
2
3
r
(b)
1.00
0.75
0.50
0.25
3.5
3.0
2.5
2.0
1.5
1.0
0.5
q_o^{-1}
1
2
3
4
5
6
b
(a_K)

Fig. 3b.

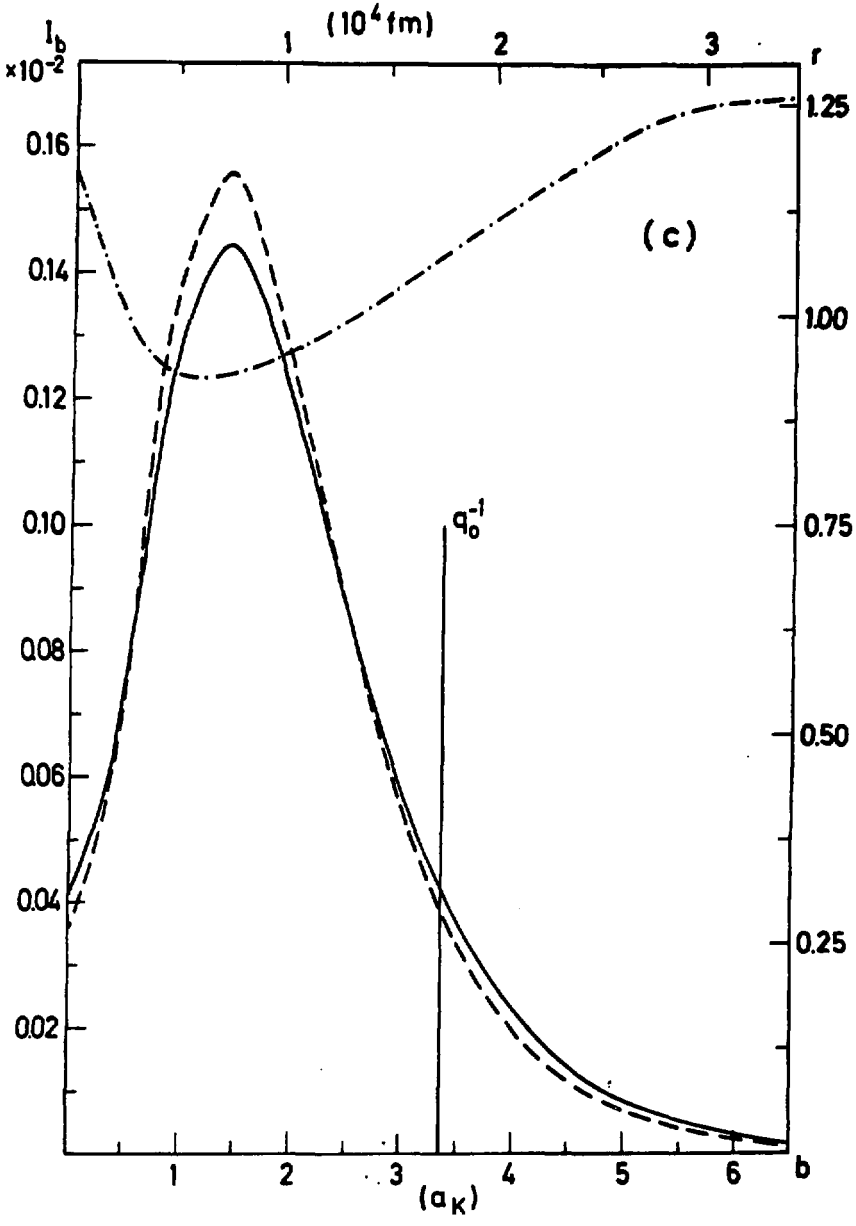

Fig. 3c.

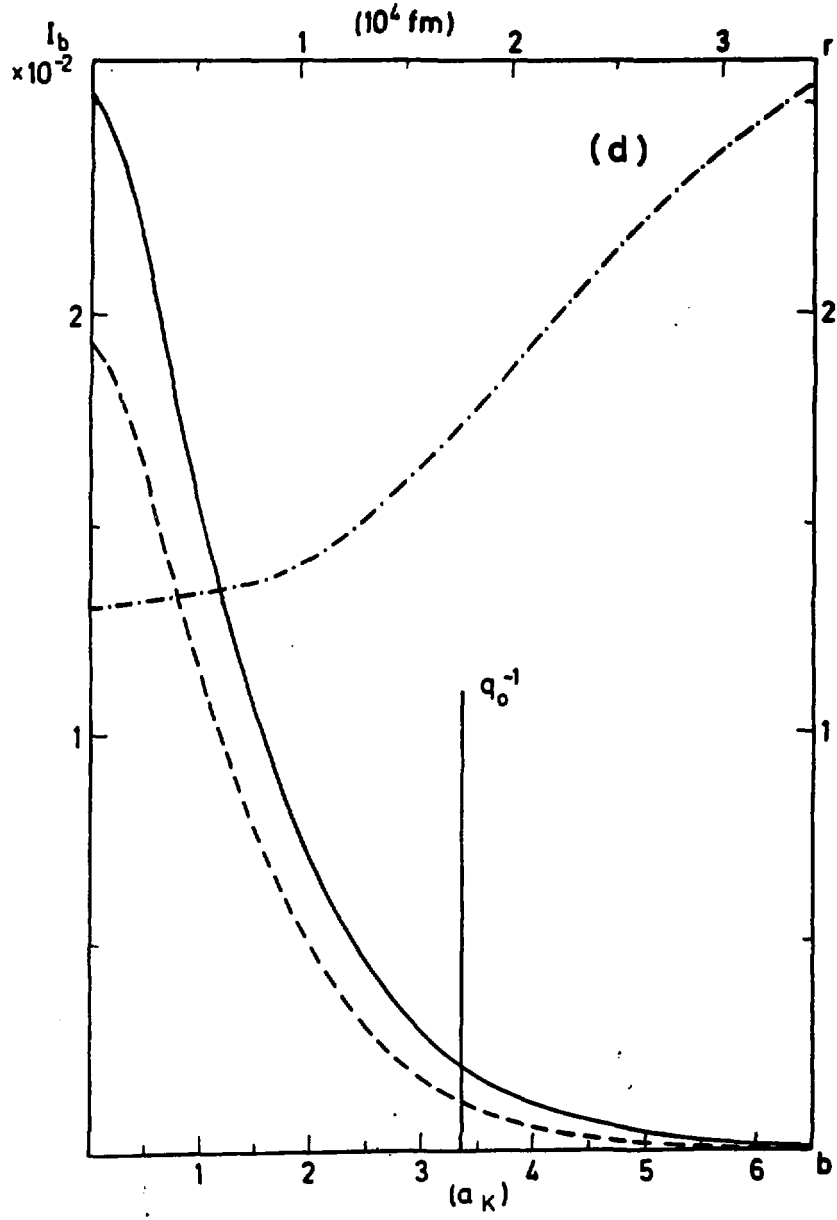

Fig. 3d.

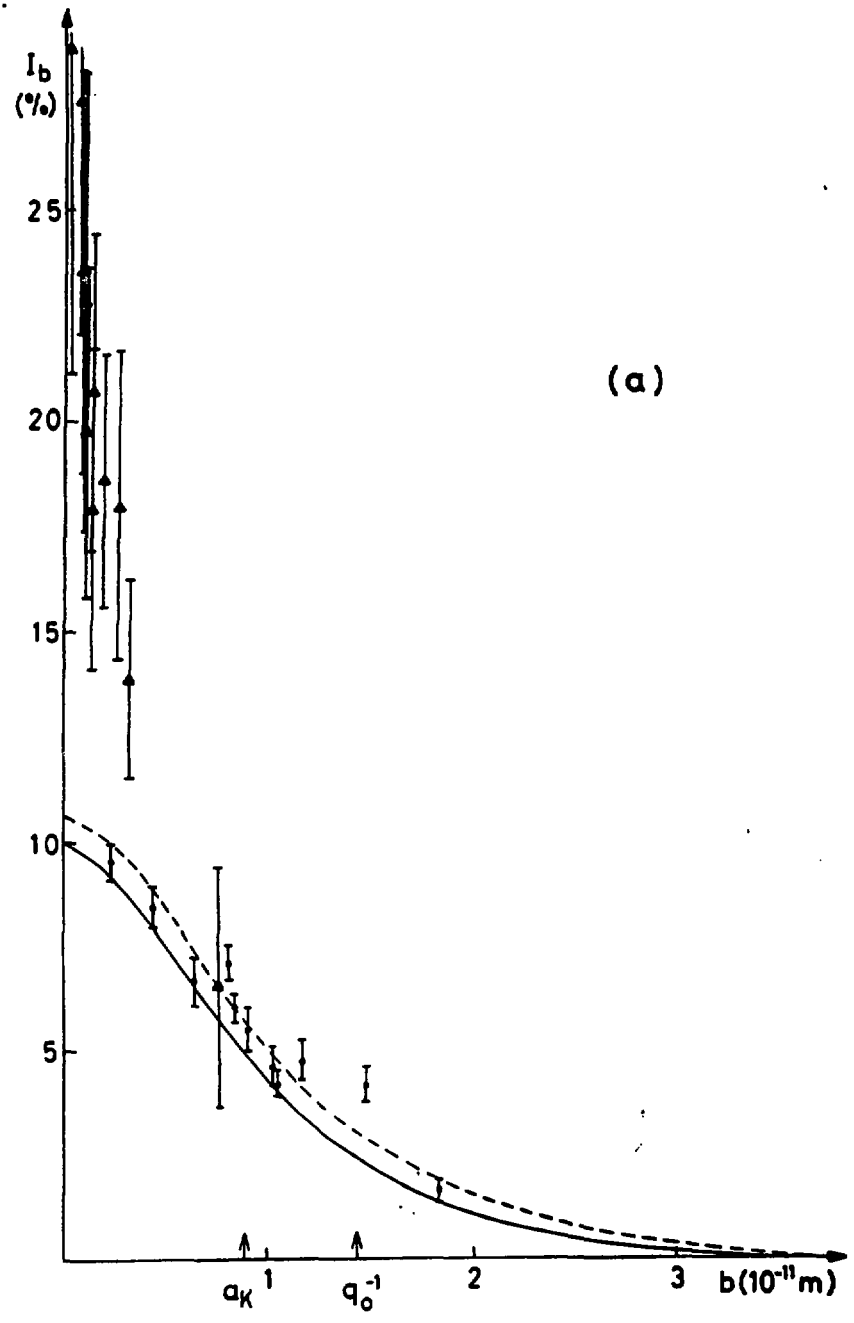

Fig. 4a.

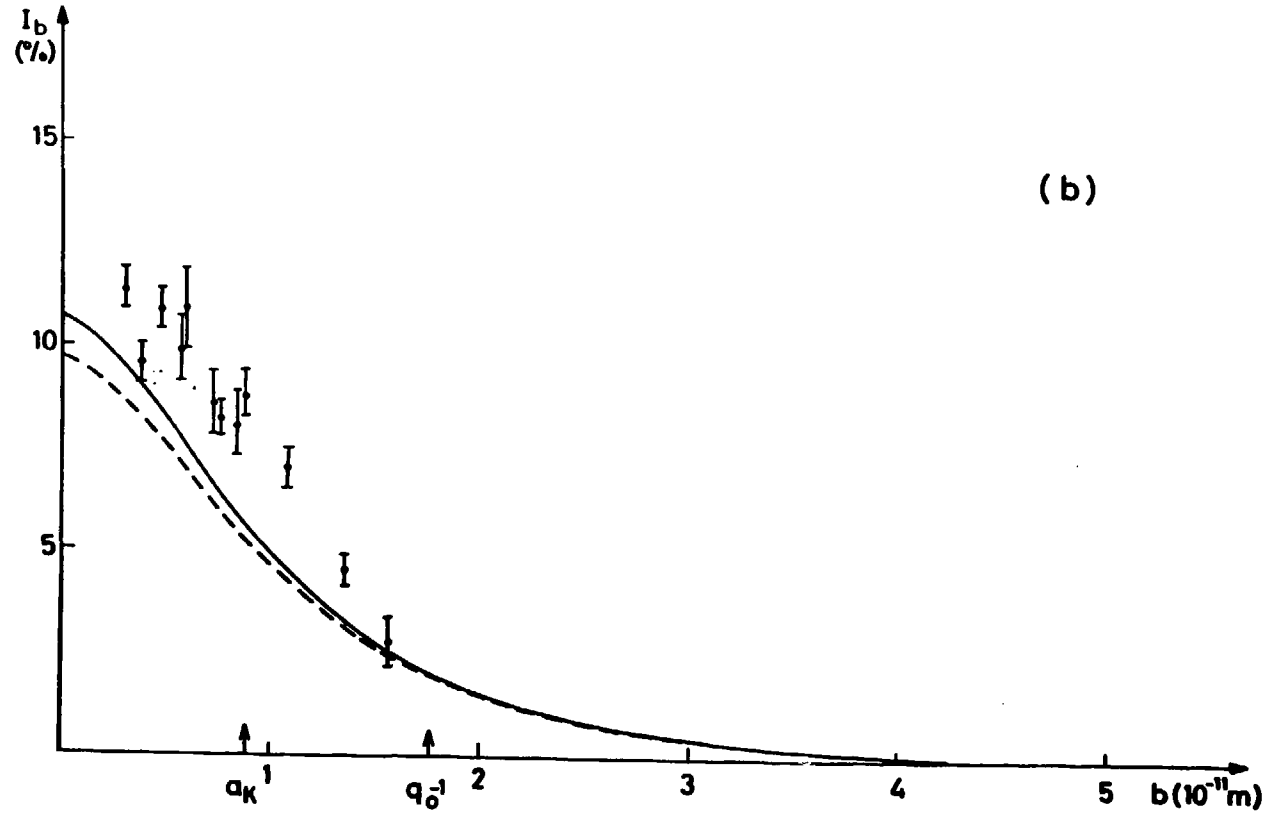

Fig. 4b.

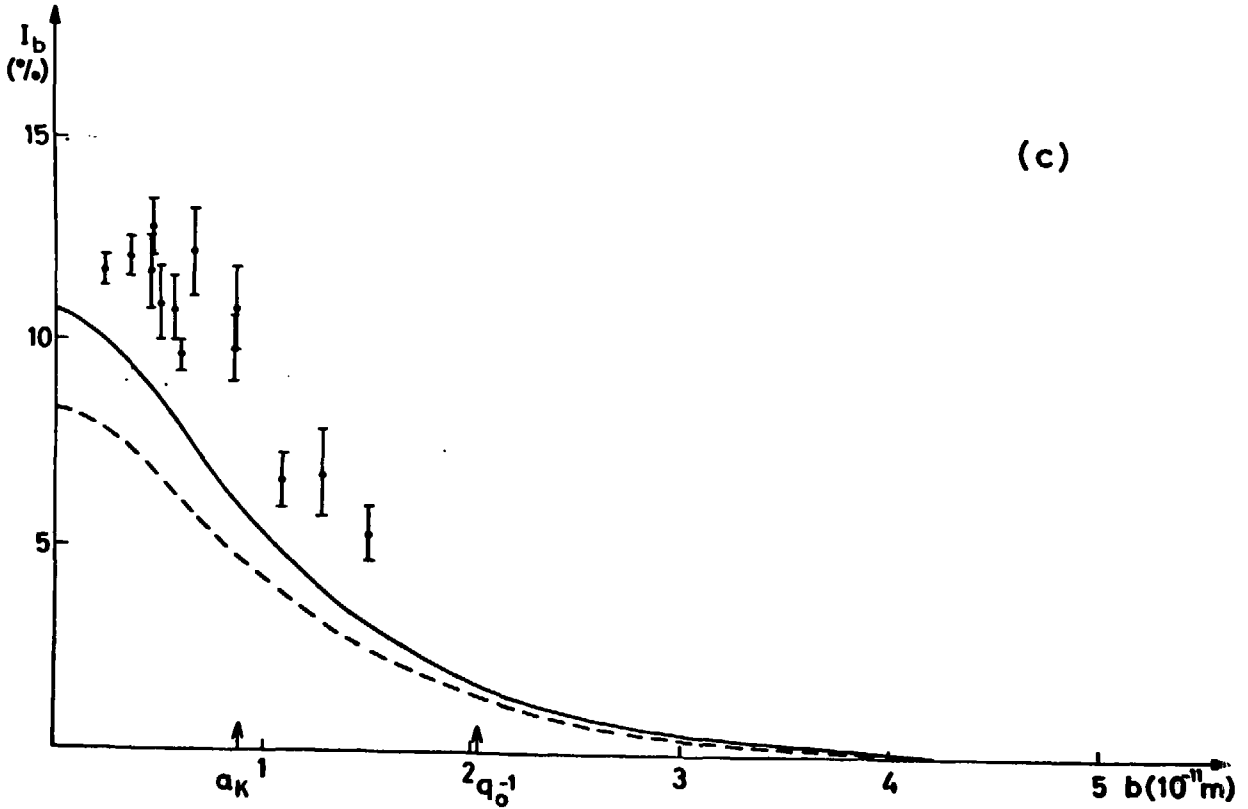

Fig. 4c.

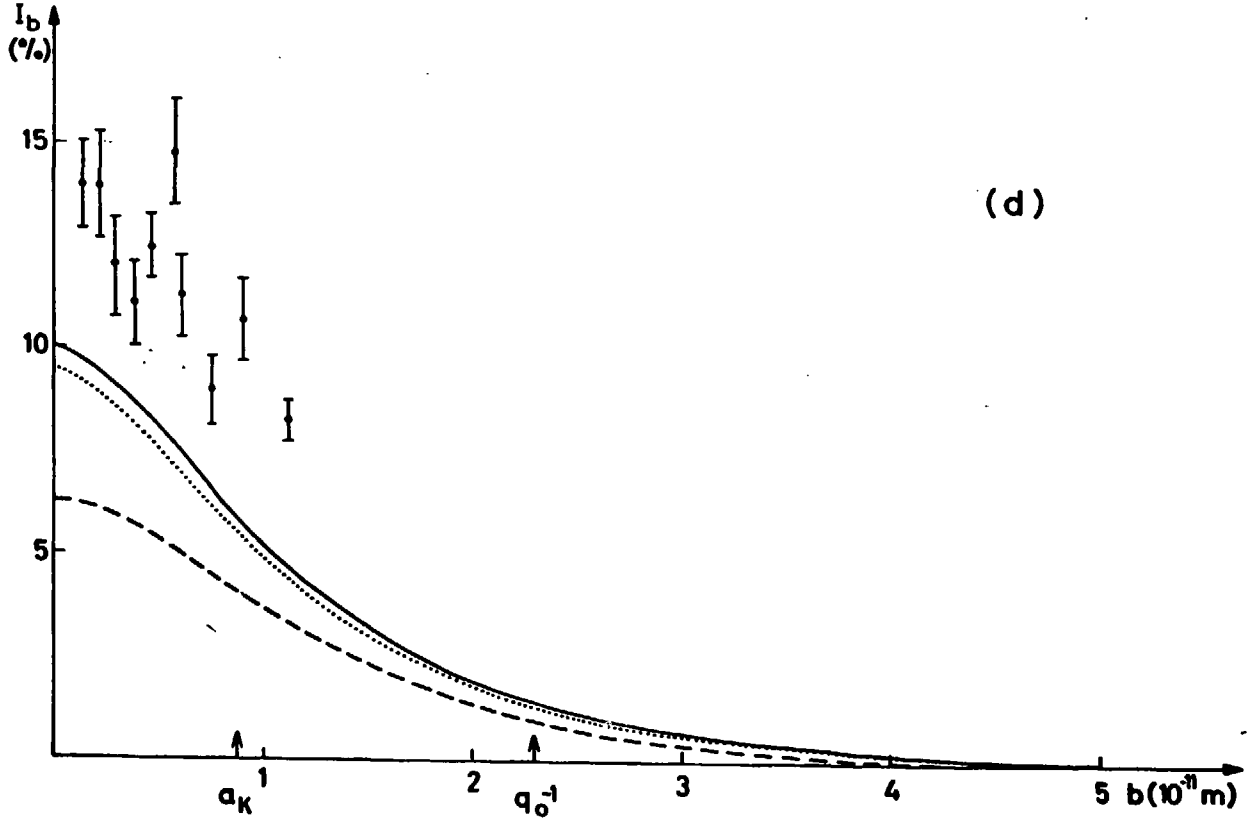

Fig. 4d.

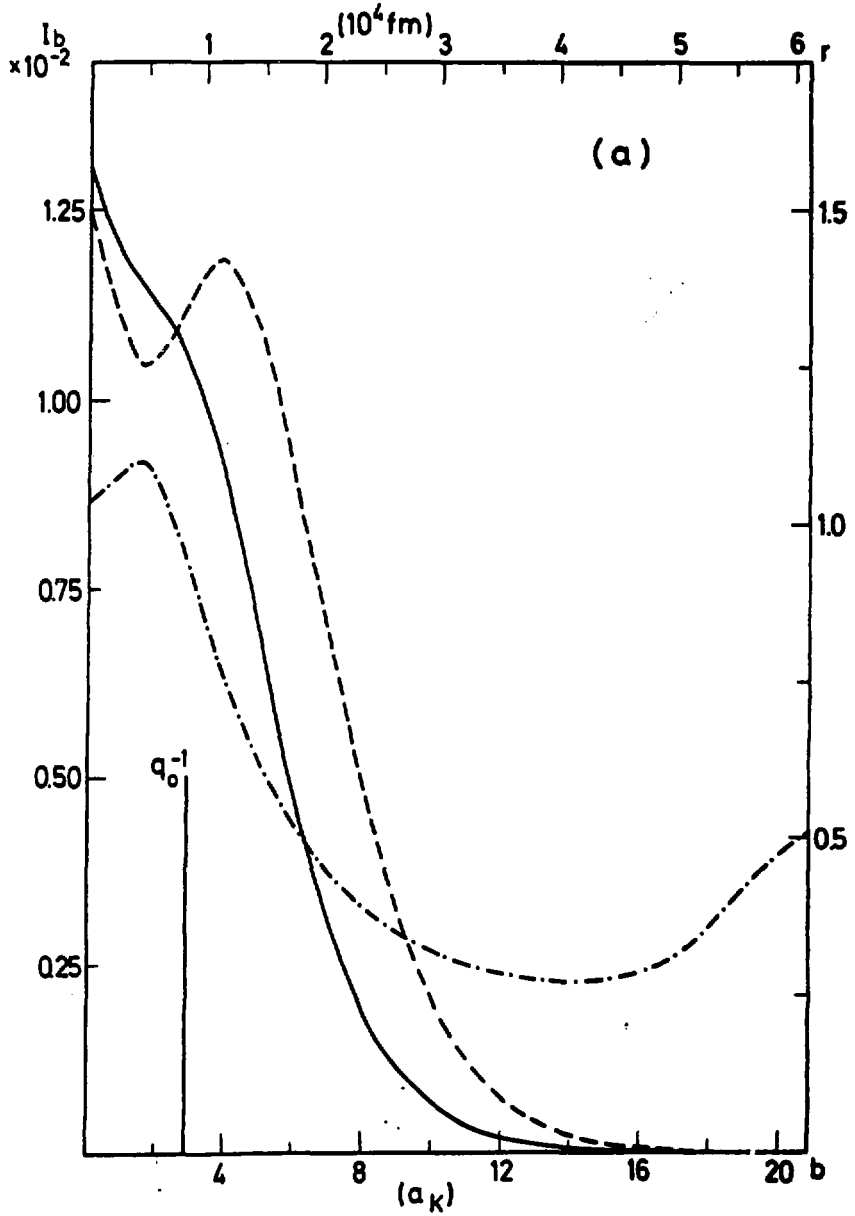
I_b
$\times 10^{-2}$
1
2
$(10^4 fm)$
3
4
5
6
r
(a)
1.25
1.00
0.75
0.50
0.25
1.5
1.0
0.5
q_o^{-1}
4
8
12
16
20
b
(a_K)

Fig. 5a.

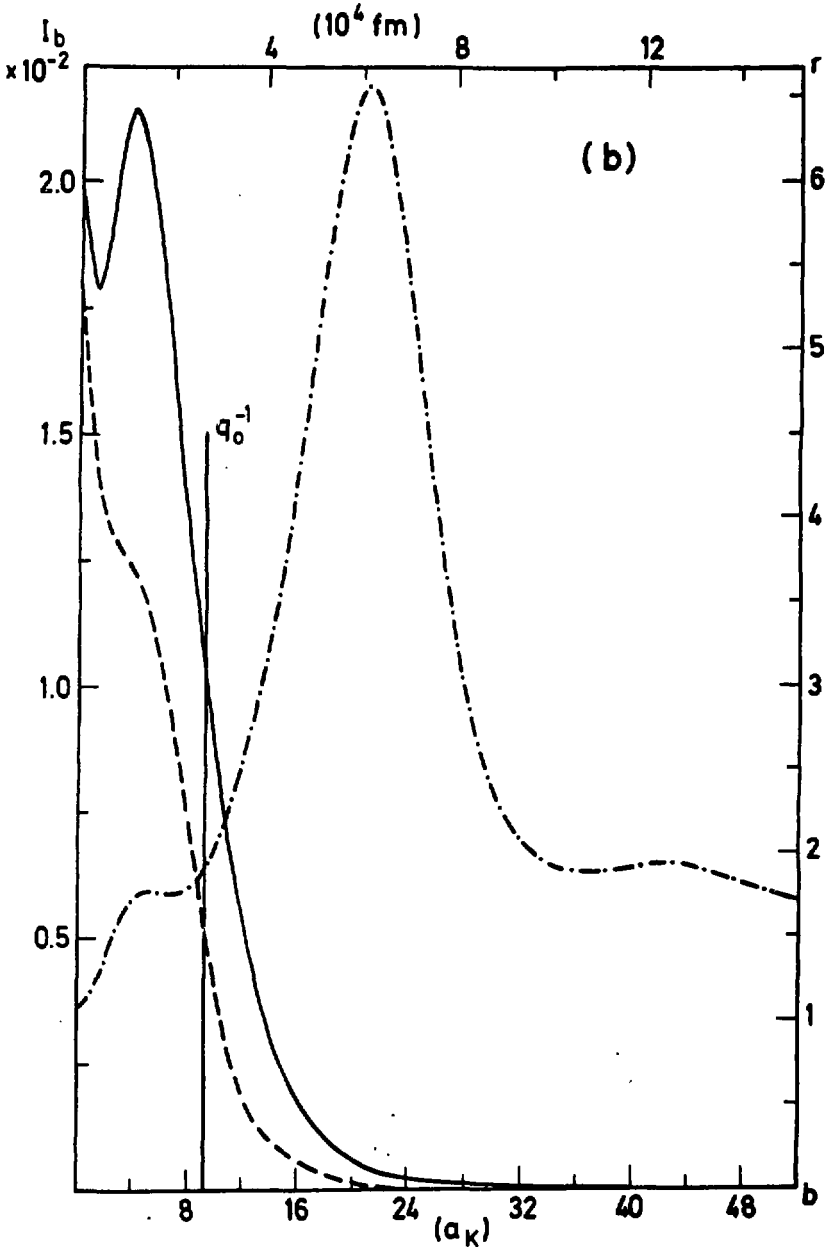
I_b
$\times 10^{-2}$
$(10^4$ fm)
4
8
12
r
(b)
2.0
1.5
1.0
0.5
q_o^{-1}
6
5
4
3
2
1
b
8
16
24
32
40
48
(a_K)

Fig. 5b.

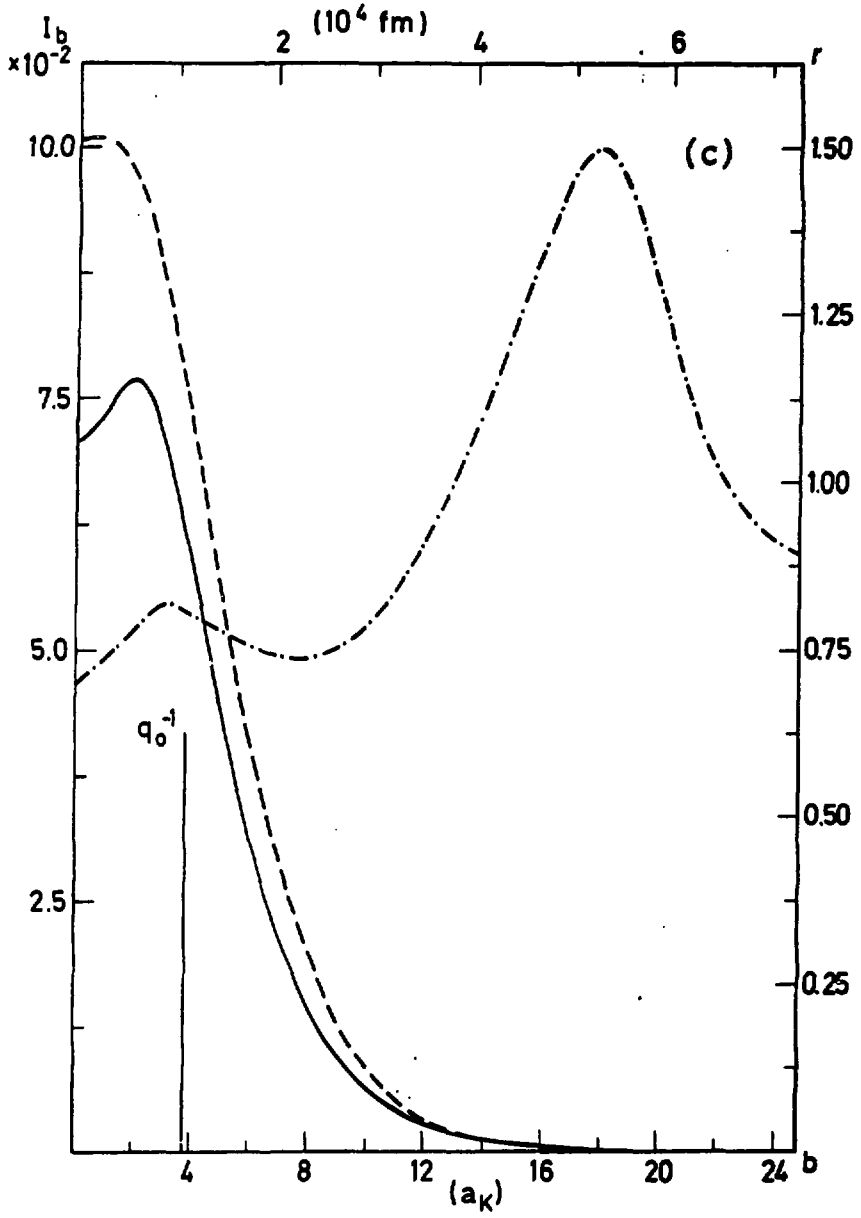
I_b
$\times 10^{-2}$
$(10^4$ fm)
2
4
6
r
10.0
7.5
5.0
2.5
(c)
1.50
1.25
1.00
0.75
0.50
0.25
q_o^{-1}
4
8
12
16
20
24
b
(a_K)

Fig. 5c.

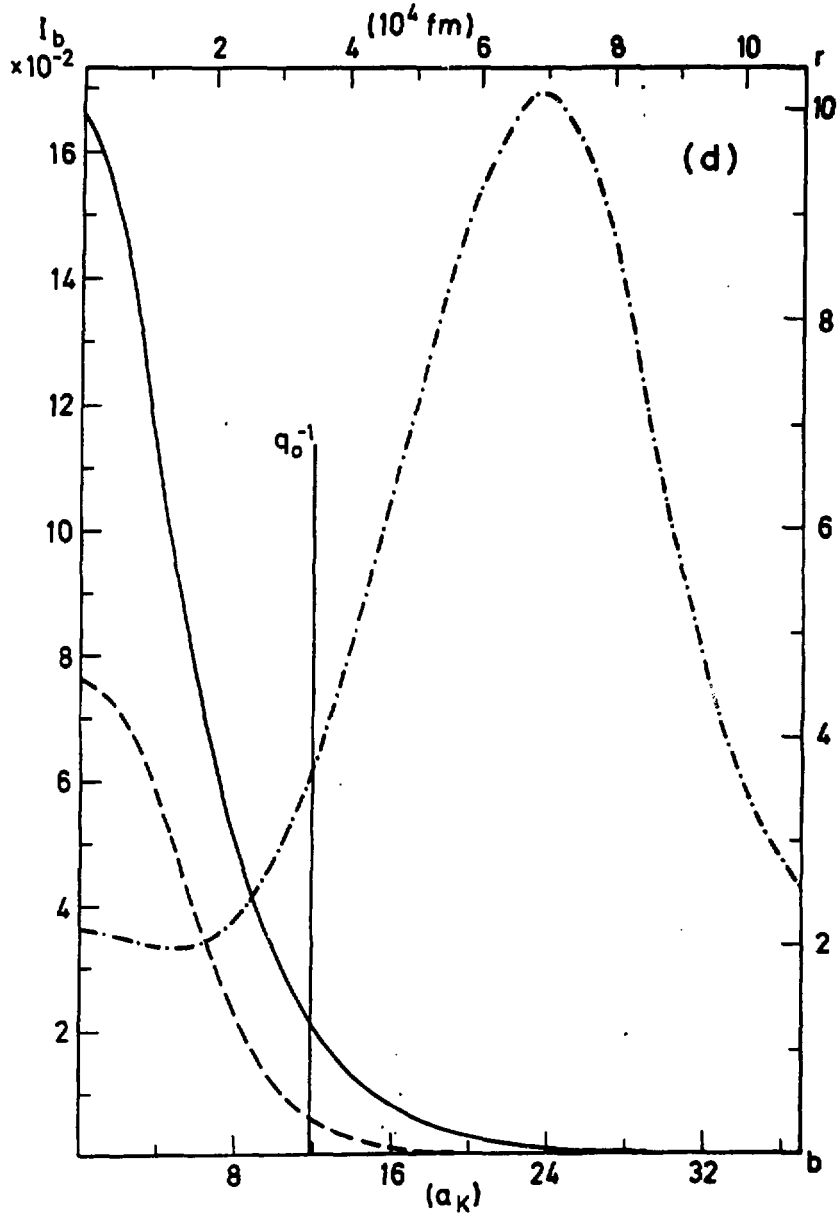
I_b
$\times 10^{-2}$
2
4
$(10^4$ fm)
6
8
10
r
16
14
12
10
8
6
4
2
(d)
q_o^{-1}
10
8
6
4
2
8
16
24
32
b
(a_K)

Fig. 5d.